อุปกรณ์รับรู้ไดมอนด์ไมโครเอทีอาร์ชนิดใหม่สำหรับการวิเคราะห์ลักษณะสมบัติเส้นใย

นางสาวฤชุวี มีชื่อ

NOVEL DIAMOND μATR SENSOR FOR

CHARACTERIZATION OF FIBERS

Miss Ruechuwee   Meechue

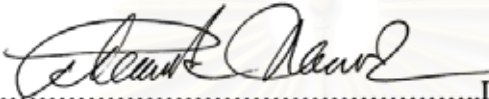A Thesis Submitted in Partial Fulfillment of the Requirements
for the Degree of Master of Science Program in Petrochemistry and Polymer Science
Faculty of Science
Chulalongkorn University
Academic Year 2005

Thesis Title Novel Diamond μATR Sensor for Characterization of Fibers

By Miss Ruechuwee Meechue

Field of Study Petrochemistry and Polymer Science

Thesis Advisor Associate Professor Sanong Ekgasit, Ph.D.

Thesis Co-advisor Associate Professor Chuchaat Thammacharoen

Accepted by the Faculty of Science, Chulalongkorn University in Partial Fulfillment of the Requirements for the Master's Degree.

……………………………………………..Dean of the Faculty of Science

(Professor Piamsak Menasveta, Ph.D.)
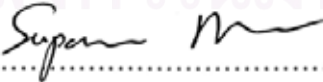
THESIS COMMITEE

…………………………………………….Chairman

(Professor Pattarapan Prasassarakich, Ph.D.)

………………………………………….Thesis Advisor

(Associate Professor Sanong Ekgasit, Ph.D.)

……………………………………….Thesis Co-advisor

(Associate Professor Chuchaat Thammacharoen)

…………………………………………….Member

(Assistant Professor Warinthorn Chavasiri, Ph.D.)

…………………………………………….Member

(Associate Professor Supason Wanichweacharungruang, Ph.D.)

ฤชุวี   มีชื่อ : อุปกรณ์รับรู้ไดมอนด์ไมโครเอทีอาร์ชนิดใหม่สำหรับการวิเคราะห์ลักษณะ สมบัติเส้นใย   (NOVEL   DIAMOND   μATR   SENSOR   FOR CHARACTERIZATION OF FIBERS) อ. ที่ปรึกษา: รศ. ดร. สนอง เอกสิทธิ์, อ. ที่ ปรึกษาร่วม: รศ. ชูชาติ ธรรมเจริญ 76 หน้า. ISBN 974-53-2712-3

อุปกรณ์รับรู้ไดมอนด์ไมโครเอทีอาร์ชนิดใหม่ใช้เพชรที่มีการเจียระไนแบบเหลี่ยมเกสรเป็น ไออาร์อีถูกพัฒนาขึ้นใช้งานร่วมกับกล้องจุลทรรศน์อินฟราเรด อุปกรณ์ชนิดใหม่นี้ให้ข้อมูลแบบ เอทีอาร์ภายใต้การสะท้อนกลับหมดของแสงภายในเพชร เนื่องจากความแข็งของเพชร ทำให้ สามารถวิเคราะห์สารตัวอย่างที่มีผิวหน้าไม่เรียบ หรือตัวอย่างของแข็งซึ่งมีปัญหาเรื่องการสัมผัส กับไออาร์อีแบบเดิม นอกจากนี้ขนาดพื้นที่ผิวสัมผัสที่มีขนาดเล็กของเพชรจึงเหมาะกับการ วิเคราะห์สารตัวอย่างที่มีขนาดเล็กมาก งานวิจัยนี้เสนอการวิเคราะห์เส้นใยเดี่ยวด้วยอุปกรณ์รับรู้ ไดมอนด์ไมโครเอทีอาร์ชนิดใหม่ เอทีอาร์สเปกตรัมที่ได้ให้ข้อมูลเชิงพื้นผิวของเส้นใย และแสดง ให้เห็นความแตกต่างของเส้นใยที่ไม่ผ่านการปรับปรุงคุณภาพและผ่านการปรับปรุงคุณภาพด้วย สารเคมี ข้อมูลที่ได้จากการวิเคราะห์ด้วยอุปกรณ์รับรู้ชนิดใหม่นี้ให้ผลเหมือนกับการวิเคราะห์ด้วย เทคนิคเอทีอาร์แบบเดิมที่นิยมและยอมรับโดยทั่วไป แต่ความเข้มของการดูดกลืนสูงกว่าเนื่องจาก เพชรสัมผัสกับเส้นใยได้อย่างมีประสิทธิภาพ

สาขาวิชา ปิโตรเคมีและวิทยาศาสตร์พอลิเมอร์ ลายมือชื่อนิสิต
ปีการศึกษา 2548 ลายมือชื่ออาจารย์ที่ปรึกษา
ลายมือชื่ออาจารย์ที่ปรึกษาร่วม

4772443023: MAJOR PETROCHEMISTRY AND POLYMER SCIENCE

KEY WORD: DIAMOND μATR / TOTAL INTERNAL REFLECTION / SINGLE FIBER

RUECHUWEE MEECHUE: NOVEL DIAMOND μATR SENSOR FOR CHARACTERIZATION OF FIBERS THESIS ADVISOR: ASSOC. PROF. SANONG EKGASIT, Ph.D., CO-ADVISOR: ASSOC. PROF. CHUCHAAT THAMMACHAROEN 76 pp. ISBN 974-53-2712-3

The novel diamond μATR sensor accessory for ATR FT-IR spectral acquisition using an infrared microscope with a gem quality round brilliant cut diamond as an IRE was fabricated. The ATR spectrum under total internal reflection phenomenon within the diamond can be collected. Since diamond is the hardest material, it can be used for characterization of rough surface, hard, and rigid samples. Due to the small sampling area of diamond tip, the small sample can be employed by the diamond μATR sensor. In this work, characterizations of single fibers by a novel diamond μATR sensor were studied. The surface information of the single fibers were achieved. The observed spectra show the different spectral features between untreated fibers and chemical-treated fibers. The spectra acquired by the novel diamond μATR sensor were similar to those acquired by the conventional ATR technique. The spectral intensity of spectra acquired by the diamond μATR sensor is better than those obtained by the conventional ATR due to the better contact.

Field of student Petrochemistry and Polymer Science   Student's signature...................

Academic year .2005.....................................   Advisor's signature.....................

Co-advisor's signature...................

ACKNOWLEDGEMENTS

CONTENTS

LIST OF FIGURES

Pages

Pages

LIST OF TABLES

LIST OF ABBREVIATIONS

ATR	Attenuated total internal reflection
FT-IR	Fourier transform infrared spectroscopy
IRE	Internal reflection element
ZnSe	Zinc selenide
KRS-5	Thallium iodide/bromide
Ge	Germanium
MSEF	Mean square electric field
MSEvF	Mean square evanescent field
MCT	Mercury-cadmium-telluride
KBr	Potassium bromide
N/A	Not available

LIST OF SYMBOLS

μ	Micron (10^{-6} m)
n	Refractive index
n_0	Refractive index of the dense medium (IRE)
n_1	Refractive index of the rarer medium
I	Light intensity
I_0	Intensity of incident beam
I_R	Intensity of reflected beam
I_S	Intensity of scattered beam
I_T	Intensity of transmitted beam
I_A	Intensity of absorbed beam
α	Angle of incidence
β	Angle of refraction
θ_c	Critical angle
A	Absorbance
R	Reflectance
d_p	Penetration depth

CHAPTER I

INTRODUCTION

Infrared spectroscopy is a particularly useful analytical methods because of the rich information of a spectrum and its variety of possibilities for sample measurement and substance preparation. To collect an infrared spectrum, various sampling technique can be employed such as transmission, reflection, reflection absorption, and attenuated total reflection techniques. The choice for sampling technique depends strongly on type of the sample (*i.e.*, solid, liquid, or gas) and the required information.

Attenuated total reflection Fourier transform infrared (ATR FT-IR) spectroscopy is one of the widely employed characterization technique. Unlike the transmission technique, ATR is the surface sensitive technique. Transmission technique presents some limitations related to the lack of surface sensitivity. In transmission experiment, light propagates throughout a whole sample. Therefore, the information obtained is the average information coming from both the surface and the bulk. The absorption contribution from the surface region is very small compared to that from the bulk. In many applications (for example, degradation studies [1-3], depth profiling [3-6], surface characterizations [7-8], and forensic analysis [9-10]), it is essential that the information coming from the bulk of the material be distinguished from that coming from the surface or interface.

1.1 ATR FT-IR Spectroscopy

Attenuated total reflection Fourier transform infrared (ATR FT-IR) spectroscopy is one of the powerful surface analysis technique. The ATR technique requires an internal reflection element (IRE) or ATR crystal of high refractive index. This technique can be applied to any sample only if the sample can be put into contact with the IRE. The basic theory for ATR FT-IR spectroscopy was first introduced by Fahrenfort and Harrick in 1960 [11-12]. When incident radiation

traveling in an optically dense medium strikes the boundary of a second medium with a relatively lower refractive index with an angle greater than the critical angle. The electromagnetic field known as the evanescent field decays exponentially within a few micrometers away from the interface into the lower refractive index medium. This electromagnetic field interacts with the material and gives absorption spectrum of surface characteristics of the material.

1.2   The Advantages of ATR FT-IR Spectroscopy

ATR is a surface sensitive technique. The spectra can be collected *in situ* and in real time. It is possible to work with small penetration depth (from 0.1 to 10 µm) [13-14] and the information of samples at different depth can be obtained from ATR spectra. ATR experiment is a nondestructive technique. The samples may be solids, liquids, or thin films. It is an excellent technique for polymer thin films because the thickness of the film is not a limited parameter.

1.3   The Limitations of ATR FT-IR Spectroscopy

To collect ATR spectral information of the sample at a greater depth, variable-angle and/or variable-IRE experiment was employed. However, ATR technique is not possible to obtain spectral information of sample greater than 10 µm, which is a problem when the chemical composition of the surface is different from the bulk.

For ATR experiment, optical contact between IRE and sample is necessary for obtaining a good spectrum. When the system does not have a suitable optical contact, there is always an air gap between the sample and the IRE. The characterization of solid samples, especially hard and rigid samples, always encounters the contact problem. The absorbance deterioration is obtained when the surface of the sample is not smooth and cannot be pressed against the IRE. If the air gap is thick enough, the spectrum of sample may not be able to be observed. Moreover, a hard and rigid sample can also damage the surface of a hard IRE when it is pressed with high pressure.

Solvent casting of polymer solution or hot pressing of polymer film onto the IRE has been employed in order to ensure the optical contact. These approaches are, however, not applicable to many types of samples (*i.e.*, surface treated polymers, polymer coatings, and insoluble polymers) since the required information may be destroyed during the sample preparation. In general practice, the application of pressure to the solid sample against the IRE is employed for improving the contact between the IRE and the solid samples [15-16]. However, this approach is not generally applicable or not appropriated for soft IREs such as ZnSe and KRS-5 because the excessive force may damage the surface of the IRE. A hard and rigid sample can also damage the surface of a hard IRE such as Ge when it is subjected to a high pressure.

1.4   The Use of Diamonds as an Internal Reflection Element

Since optical contact between an IRE and a sample is crucial for obtaining a good spectrum in ATR experiment, a diamond IRE is employed for the improvement of the contact. The diamond accounts for its hardness and physical strength, it is not damage when sampling the hard and rigid samples, therefore good optical contact is obtained. Moreover, it is chemically inert. The development of diamond as an IRE opened up a number of applications in the infrared spectroscopy.

The use of diamond for ATR is not new, as a diamond microassembly was available for the Wilks Scientific model 76 ATR accessory back in 1977. Later, in 1992, a cylindrical ATR flow cell system was introduced for on-line industrial measurement. In both cases, the sampling devices were targeted at specific implementations and sample types. In 1994, a new ATR sampling technology featuring a diamond optical interface to the sample, incorporated into immersion probe, known as the DiComp Probe, was introduce for process analysis applications [17].

In 1995, a new micro-ATR accessory was introduced, called the DurasamplIR (SensIR Technologies, CT, USA) [18-19]. In its standard form, this accessory features a diamond IRE sampling surface. All the practical benefits of diamond are

retained: its strength and chemical inertness, and good optical performance with minimum interference in the region of the diamond absorption. This arrangement is made practically by a unique combination of a small, thin diamond element placed on top of a larger optical element made from a material of comparable refractive index, usually zinc selenide. The second, larger element acts as a mechanical support and as focusing device for the infrared entering and exiting the diamond IRE. However, on a larger optical element placed by thin diamond element has the limitation of hardness. If high pressure is applied, it will break or crack. Moreover, the commercial DurasamplIR is expensive.

Recently, various commercial diamond ATR accessories are available. However, most of the commercial diamond IREs were specially designed and built-in the ATR objective. With a small surface area it is exerted a significant force with minimal applied pressure. They are dangerous when the application is associated with over-pressurisation. In extremely cases, with hard materials and too much applied pressure, there is a risk to crack the diamond.

From the limitations of commercial diamond ATR accessories, the homemade diamond μATR sensor accessory was developed by the Sensor Research Unit, Department of Chemistry, Faculty of Science, Chulalongkorn University. A gem quality round brilliant cut natural diamond was employed as an IRE [20]. The novel diamond IRE has two configurations; a sharp-tip (*i.e.*, a faceted diamond with a very small culet) and flat-tip (*i.e.*, a faceted diamond with an expand culet) for various types of the required information. In this work the flat-tip diamond IRE was approximately 0.1 mm in diameter. The diamond IRE was impermanent mounted into the probing head, therefore, it is very easily to clean the IRE. Moreover, the homemade diamond μATR accessory is cost effective. The novel diamond μATR sensor can apply in various materials such as hard and rigid [20], rough surface, irregular shape samples, small sample, and good optical contact between sample and IRE is obtained as well. The spectral information at greater depth can be acquired by simply applying pressure on the sample against the culet of the sharp-tip diamond IRE. Due to the optical transparency of the diamond, the image of the sample attached to the flat-tip diamond IRE can be visualized though an optical microscope.

Therefore, a small sample or a small area on the surface of the sample can be selectively observed.

1.5   The Objective of This Research

The objective of this research is to develop the accessory of novel diamond µATR sensor and characterization of single fibers by a novel diamond µATR sensor. ATR spectra obtained by novel technique will be compared with spectra obtained by the conventional ATR.

1.6   The Scope of This Research

1. To design and to improve the accessory of novel diamond µATR sensor.
2. To characterize the fibers by a novel diamond µATR sensor.
3. To compare infrared spectra observed by novel diamond µATR sensor with those obtained by the conventional ATR.

CHAPTER II

THEORETICAL BACKGROUND

2.1 Fundamentals of Light Propagation

Light is by nature an electromagnetic wave produced by the vibration of an electric charge. In its simplest monochromatic form, light can be represented as polarized, oscillating electric and magnetic fields that propagate in space, as depicted in Figure 2.1 [21]. The electric and magnetic vectorial components are orthogonal to each other and to the direction of propagation.
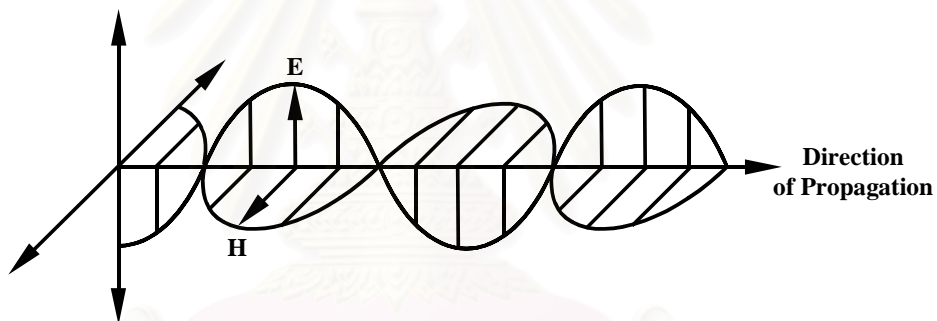
Figure 2.1 Propagation of a linearly polarized electromagnetic wave in the direction of propagation. The electric (**E**) and magnetic (**H**) vectorial components are orthogonal to each other and to the direction of propagation. In unpolarized light, the electric component **E** is randomly oriented in an infinite number of directions, but remains always perpendicular to the direction of propagation.

When such an electromagnetic radiation impinges on a specimen, rays of the incident beam may be reflected, scattered, transmitted, or absorbed. Depending on the experimental arrangements, various rays may be detected. The total amount of incident energy is the sum of reflected, scattered, transmitted, and absorbed light. A

schematic illustration for an interaction between light and matter is illustrated in Figure 2.2. This process can be expressed by the following relationship [21]:

$$I_0 = I_R + I_S + I_T + I_A \tag{2.1}$$

where I_0 is the intensity of the incident beam and I_R, I_S, I_T, and I_A are the intensities of reflected, scattered, transmitted, and absorbed beams, respectively. The intensity of each beam depends on the intensity and wavelength of the incident radiation, the optical properties of the specimen, the concentrations of species, and the geometry of the experimental setup.

Elastic or inelastic
scattering (I_S)

Incident Beam ——— **Reflected** ←———→ **Transmitted (I_T) Beam**
(I_0) **Beam**
(I_R)
Sample
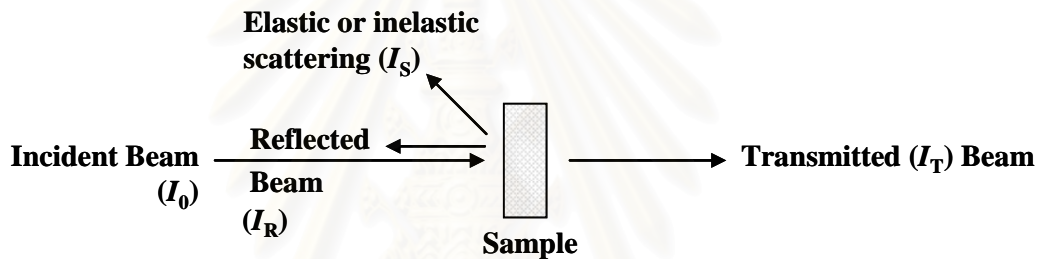
Figure 2.2   Interactions of light with matter.

Considering, the electromagnetic radiation when a sample is inserted between a source of light and a detector, as seen in Figure 2.2. The sample absorbs a fraction of the incident radiation. We will neglect reflection and scattering and measure the amount of light transmitted by the sample. For that purpose we need to measure the ratio of the sample attenuated (I) and nonattenuated (I_0) intensities of the radiation. The ratio is proportional to the transmittance of the sample. This relationship can be quantitatively related to the chemical composition of the sample by the Beer-Lambert law as [21]:

$$I / I_0 = e^{-A(v)} = e^{-c_2 \varepsilon(v) l} \tag{2.2}$$

where $A(\nu)$ is the sample absorbance at a given wavenumber ν, c_2 is the concentration of the absorbing functional group, $\varepsilon(\nu)$ is the wavenumber-dependent absorption coefficient, and l is the film thickness for the infrared beam at a normal incidence to the sample surface.

A simple transmission experiment as described above may provide a significant amount of information concerning molecular structures and their properties. One apparently drawback is that the technique is not applicable to surface analysis. If one wants to gain an insight understanding of the surface properties such as chemical compositions, molecular orientation, and chemical reaction, a surface sensitive technique is required. ATR FT-IR is a good candidate for this purpose. It is not only a technique that provides the information, which directly associated to chemical composition of the sample but also a surface sensitive technique.

2.2   Principles of Light Reflection and Refraction

When an electromagnetic radiation strikes a boundary between two media with different refractive indices, refraction and reflection occur. The law that governs the reflection process requires that the angle of incidence is equal to the angle of reflection. In this case, reflection is specular. If electromagnetic radiation passes from one medium to another that has a different refractive index, a sudden change of beam direction takes place because of the differences in propagation velocity through two media. If light propagates through an incident medium with refractive index n_0 and enters a medium with refractive index n_1 (Figure 2.3), the light path will be changed and the extent of refraction is given by the following expression, known as Snell's law [21]:

$$n_0 \sin \alpha = n_1 \sin \beta \qquad (2.3)$$

where α and β are the angles of incidence and refraction, respectively.
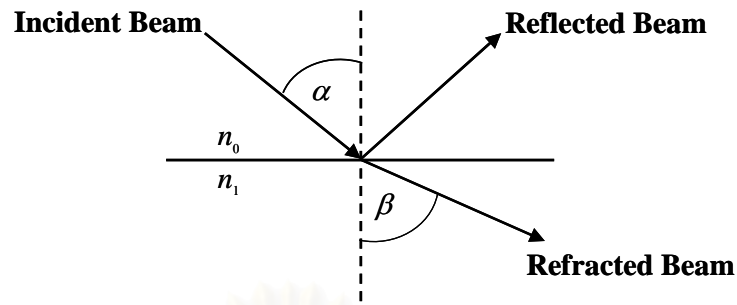
Figure 2.3   Reflection and refraction of a plane wave at a dielectric interface based on Snell's Law.

Total internal reflection occurs when light traveling in an optically denser medium impinges on surface of a rarer medium (*i.e.*, $n_0 > n_1$) with an incident angle greater than the critical angle. The critical angle can be derived from Snell's law and given by Equation 2.4. As illustrated in Figure 2.4, when the angle of the incidence equals the critical angle, θ_c, the refracted angle equals 90°. This implies that under a total internal reflection phenomenon there is no light from the optically denser medium travels across the interface into the optically rarer medium.

$$\theta_c = \sin^{-1}(n_1 / n_0) \qquad\qquad (2.4)$$

where n_0 and n_1 are the refractive indices of the denser medium and that of rarer medium, respectively.
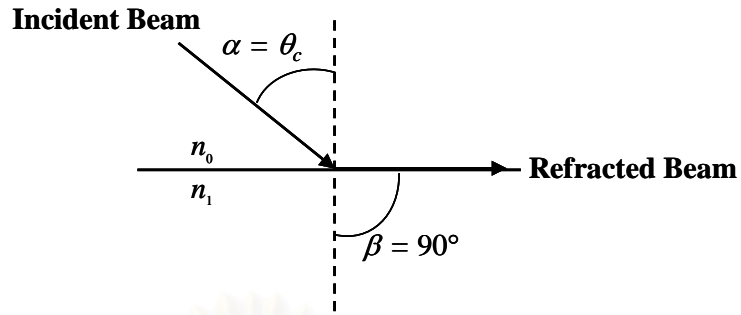
Figure 2.4 Condition under which total internal reflection occurs. Light travels from an optically denser medium and impinges at the surface of the optically rarer medium ($n_0 > n_1$) at an angle equal critical angle.

2.3 ATR FT-IR Spectroscopy

ATR FT-IR spectroscopy stands for attenuated total reflection Fourier transform infrared spectroscopy. It is a material characterization technique using an internal reflection principle. The total internal reflection is an optical phenomenon, which can be observed easily, for example, with a glass of water. If the side of the glass below the water level is viewed obliquely through the water surface, it appears to be completely silvered and one can no longer see objects behind it. The reason for this is that light striking the glass surface is totally reflected and therefore does not pass through the surface in order to illuminate these objects.

In an ATR configuration, a denser medium (*i.e.*, an internal reflection element, IRE) is optically contacted with rarer medium (*i.e.*, a sample) as shown in Figure 2.5. The IRE is infrared transparent and has a refractive index n_0. The sample is infrared absorbing and has a complex refractive index at frequency v (cm^{-1}) of [21]:

$$\hat{n}_1 = n_1 + ik_1 \tag{2.5}$$

where n_1 and k_1 are refractive index and absorption index, respectively.
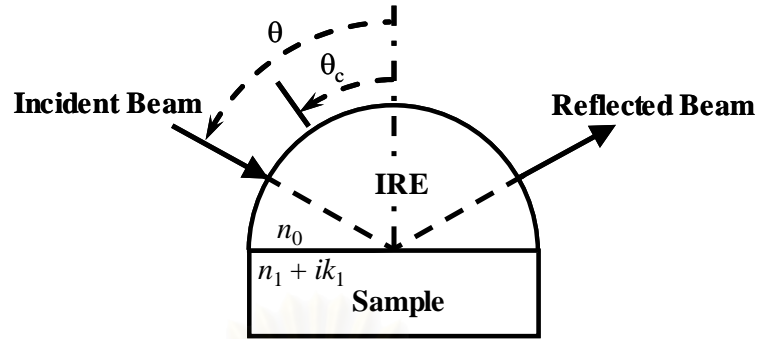
Figure 2.5   Ray tracing under total internal reflection.

Incident light travels from the IRE and impinges the IRE/sample interface with an incident angle greater than the critical angle. Under non-absorbing condition (i.e., the rarer medium is transparent or absorption index of the medium equals zero), the incident light is totally reflected at the interface. Since there is no light travel across the interface, no reflection loss due to absorption is observed. This phenomenon is defined as total reflection phenomenon. When the rarer medium is absorbing (*i.e.*, its absorption index is greater than zero), there is a reflection loss due to absorption by the sample. Reflectance of the beam leaving IRE/sample interface is less than unity. This phenomenon is defined as attenuated total reflection (ATR) phenomenon.

Although no light travels across the boundary, there is a strong electric field at the interface region of the IRE/sample. This electric field known as the *evanescent field*, decays exponentially within a few micrometers from surface of the IRE. Interaction between the evanescent field and the sample is the cause of reflection loss in ATR experiments.

2.3.1   Internal Reflection Elements (IRE)

The internal reflection element (IRE) is an infrared transparent material used in internal reflection spectroscopy for establishing the conditions necessary to obtain internal reflection spectra of materials. In general, the IRE configuration included variable-angle hemispherical crystal with single reflection and multiple reflection planar crystal (Figure 2.6). ATR spectra are easily obtained by placing the sample

against the IRE while the infrared radiation is coupled into the IRE. The information obtained from the spectrum depend on several factors such as properties of IRE, angle or range of angles of incidence, number of reflections, aperture, number of passes, surface preparation, and material from which it is made [13].

A. Single Reflection   **B. Multiple Reflection**
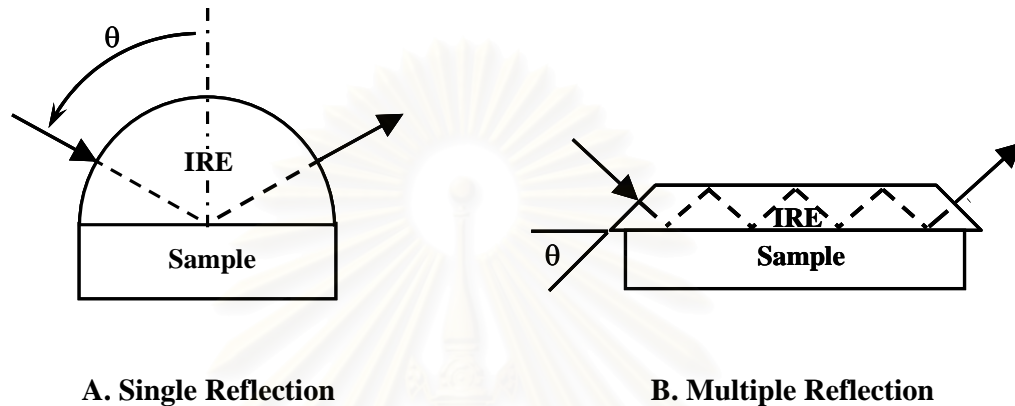
Figure 2.6   Selected IRE configurations commonly used in ATR experimental setups: single reflection variable-angle hemispherical crystal (A), and multiple reflection single-pass crystal (B).

2.3.2   ATR Spectral Intensity

In ATR experiment, the magnitudes of the interaction between light and the sample can be expressed in terms of absorbance. The absorbance depends on both the material properties (e.g., refractive index of the IRE and complex refractive index of the sample) and the experimental parameters (e.g., angle of incidence and polarization of the incident beam). The relationship between absorbed and reflected intensity in an ATR spectrum is given by [22]:

$$A_l(\theta, v) = 1 - R_l(\theta, v) \tag{2.6}$$

where $A(\theta, v)$ and $R(\theta, v)$ are absorptance and reflectance, respectively and l indicates the polarization of the incident beam. The polarization direction is given with respect to the plane of incidence. The plane of incidence is defined as the plane that contains both incident and reflected beam. For p-polarization (p- stands for

parallel), the electric component of the electromagnetic wave is parallel to the plane of incidence while the magnetic component is perpendicular to the plane of incidence. The electric component of the electromagnetic wave with *s*-polarization (*s*- stands for senkrecht) is perpendicular to the plane of incidence while the magnetic component is parallel to the plane of incidence. In general, absorptance in ATR can be expressed in terms of experimental parameters and material characteristic by the following expression [21]:

$$A_{\bar{p}}(\theta,v) = \frac{4\pi v}{n_0 \cos\theta} \int_0^\infty n_1(v) k_1(v) \langle E_z^2(\theta,v) \rangle dz \qquad (2.7)$$

where $\bar{p}$ indicates degree of polarization of the incident beam, $\langle E_z^2(\theta,v) \rangle$ is the mean square electric field (MSEF) at depth z. $n_1(v)$, and $k_1(v)$, respectively, are the refractive index and absorption index of the sample, and n_0 is the refractive index of the IRE. The MSEF has the strongest in magnitude at the IRE/sample interface. Its strength decreases exponentially as a function of depth. The MSEF is, however, also a function of experimental condition and material characteristics.

Under the ATR condition, although there is no light travels across the IRE/sample interface, there is an evanescent field generated at the boundary. This field is strongest at the interface and exponentially decays as a function of distance from the interface. The rapid decay of the evanescent field is the unique characteristic of technique that makes ATR as a powerful surface characterization. The decay pattern of the evanescent field can be expressed in terms of the distance from IRE/sample interface by the follow expression [13]:

$$\langle E_z^2(\theta,v) \rangle = \langle E_0^2(\theta,v) \rangle e^{-2z/d_p(\theta,v)} \qquad (2.8)$$

where $d_p(\theta,v)$ is the penetration depth. $\langle E_0^2(\theta,v) \rangle$ and $\langle E_z^2(\theta,v) \rangle$ are the mean square evanescent filed at the interface and the depth z, respectively. The evanescent

field characteristic at the boundary between the IRE and the sample is shown in Figure 2.7 [13].
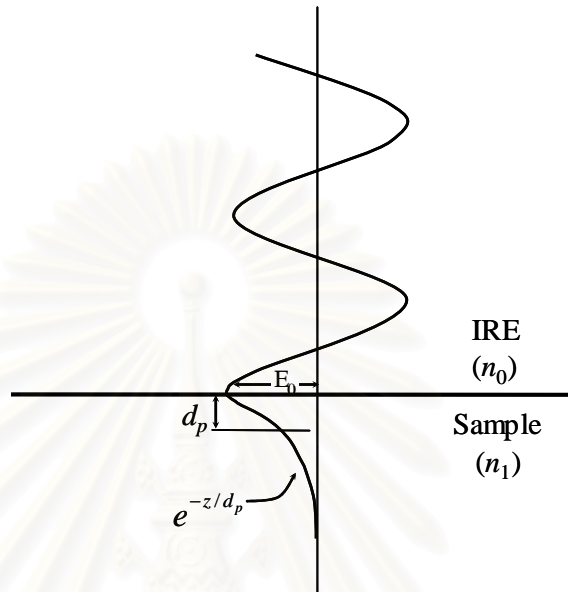
Figure 2.7   The evanescent field at the boundary between the IRE and the sample.

The penetration depth is defined as the depth where the electric field strength decays to 1/e of its value at the interface. The penetration depth is given in term of material characteristics and experimental parameter by:

$$d_p = \frac{1}{2\pi v n_0 \left(\sin^2 \theta - (n_1/n_0)^2\right)^{1/2}} \tag{2.9}$$

where v is the frequency of the infrared radiation and θ is the angle of incidence. By the altering the angle of incidence while ensuring that it remains larger than the critical angle, the depth of penetration is consequently varied. Example of the penetration depth at various experimental conditions and material characteristics are shown in Figures 2.8 and 2.9.
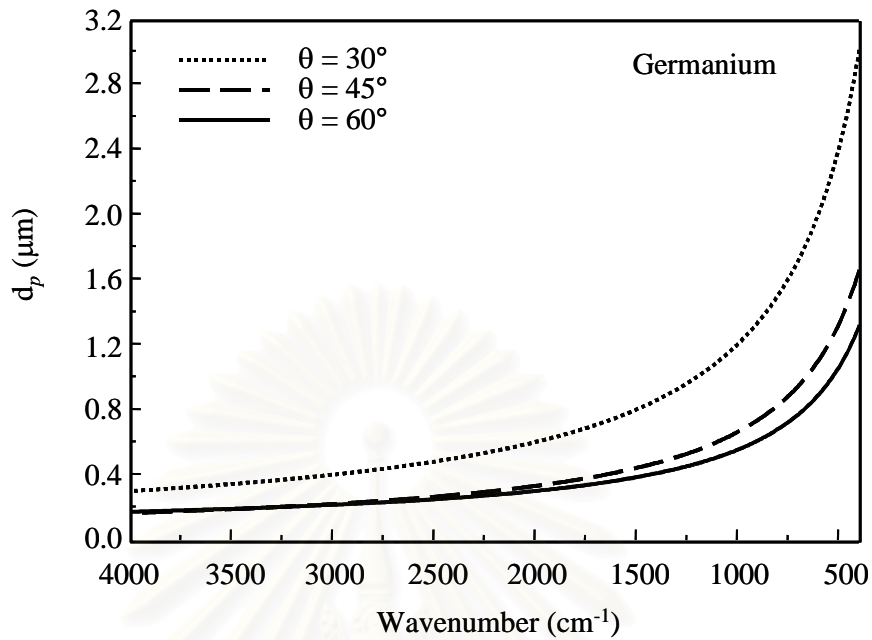
Figure 2.8   Relationship between the penetration depth and wavenumber for Ge crystal ($n_0 = 4.0$) at different angle of incidence.
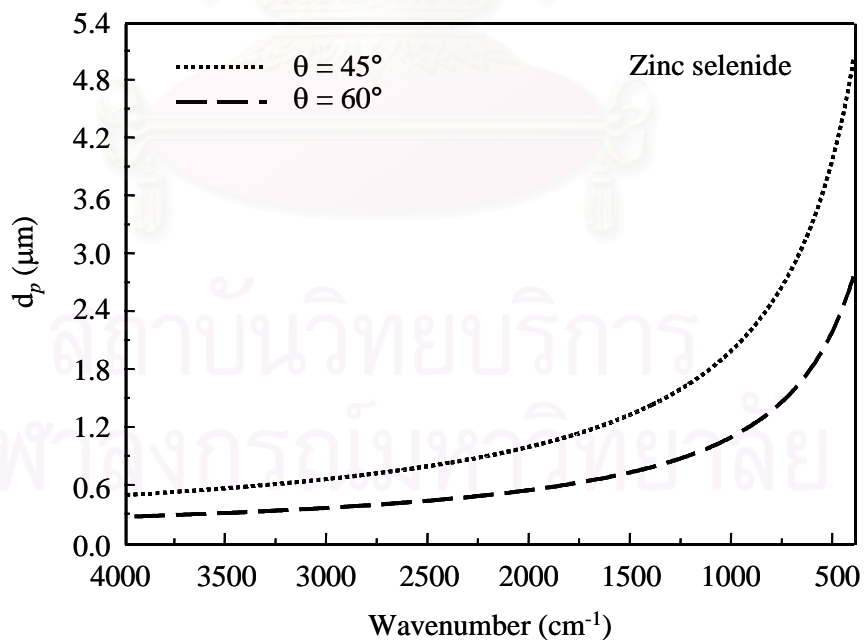
Figure 2.9   Relationship between penetration depth and wavenumber for ZnSe crystal ($n_0 = 2.4$) at different angle of incidence.

Figure 2.8 and 2.9 show that the penetration depth depends strongly on experiment conditions and material characteristic. Under a non-absorbing condition (*i.e.*, $k_1(v) = 0$), the MSEF can be calculated if the refractive index of material is known. Under this condition, the MSEF is given a special name as the mean square evanescent field (MSEvF). The strength and the decay characteristic of the MSEvF can be given in a much simpler than those of MSEF. The MSEvF at the interface with *p*- and *s*-polarized radiation is given, respectively, by [13]:

$$\left\langle E_{p,z=0}^2(\theta,v) \right\rangle_{k=0} = \frac{4\cos^2\theta\left[\sin^2\theta - \left(n_1(v)/n_0\right)^2\right] + 4\cos^2\theta\sin^2\theta}{\left[1 - \left(n_1(v)/n_0\right)^2\right]\left\{\left[1 + \left(n_1(v)/n_0\right)^2\right]\sin^2\theta - \left(n_1(v)/n_0\right)^2\right\}} \quad (2.10)$$

$$\left\langle E_{s,z=0}^2(\theta,v) \right\rangle_{k=0} = \frac{4\cos^2\theta}{1 - \left(n_1(v)/n_0\right)^2} \quad (2.11)$$

The field strength and decay characteristics of the MSEF significantly deviate from those of MSEvF as the absorption index become larger (*i.e.*, large absorption index and small angle of incidence). The influence of absorption on the field characteristics is more pronounced in the case of IRE with low refractive index such as ZnSe. The MSEF at various conditions are shown in Figure 2.10.
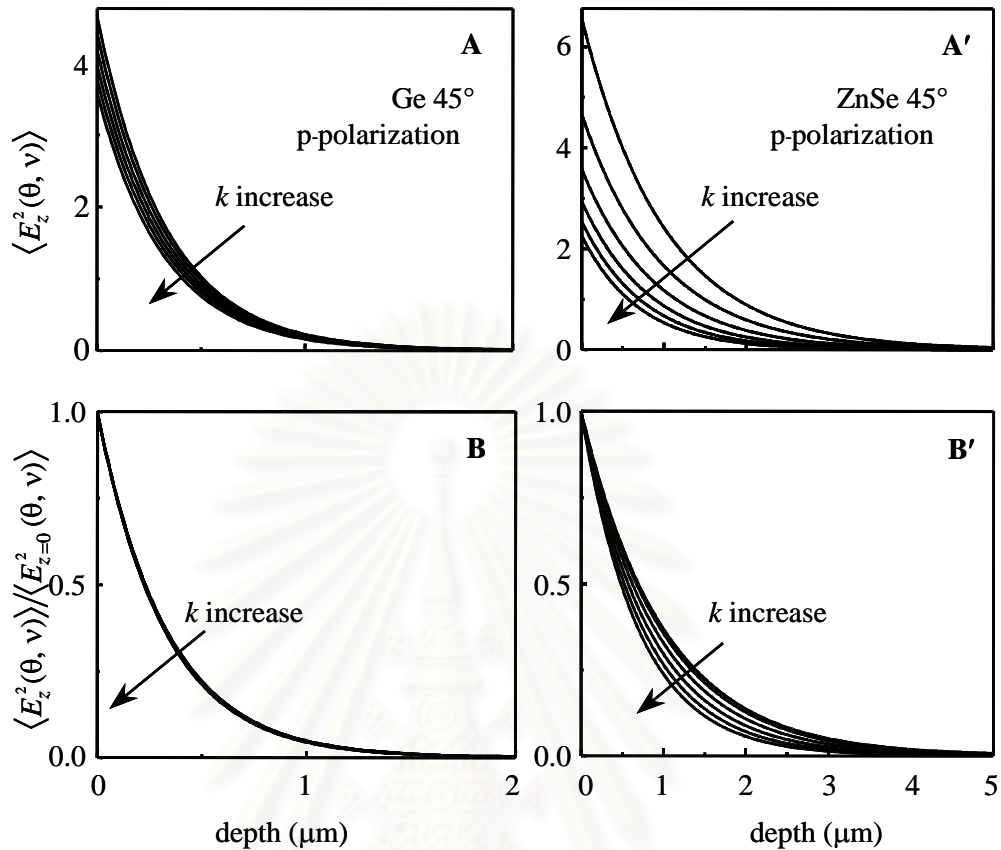
Figure 2.10 The MSEF at various experimental condition (A, A′) and its decay characteristic (B, B′). The simulation parameters are $n_0 = 4.00$ for Ge, $n_0 = 2.40$ for ZnSe, $v = 1000$ cm^{-1}, $n_1(v) = 1.50$, $k_1(v) = 0.0, 0.1, 0.2, 0.3, 0.4$, and 0.5, respectively.

According to equations 2.9-2.11, the MSEvF at any depth can be calculated if the reflective index is known. Unlike the MSEvF, the MSEF can be obtained only if the complex refractive index of the material is known. However, this is not usually the case since the complex refractive index of a material is not generally available. Under a weakly absorbing condition (*i.e.*, the absorption index is small and the angle of incidence is much greater than the critical angle), the strength and the decay characteristics of the MSEF are similar to those of the MSEvF. The MSEF can accurately be estimated from the MSEvF by the following expression:

$$\left\langle E_z^2(\theta,v) \right\rangle = \frac{1+R(\theta,v)}{2} \left\langle E_z^2(\theta,v) \right\rangle_{k=0} \qquad (2.12)$$

where $R(\theta,v)$ is reflectance and $\left\langle E_z^2(\theta,v) \right\rangle$ and $\left\langle E_z^2(\theta,v) \right\rangle_{k=0}$, respectively, are the MSEF and MSEvF at depth z.

By substituting Equations 2.9 and 2.12 into Equation 2.7, the absorption in ATR spectroscopy, under a weakly absorbing condition, can be expressed in terms of the MSEvF by the following expression:

$$A(\theta,v) = \frac{1+R(\theta,v)}{2} \cdot \frac{4\pi v \left\langle E_0^2(\theta,v) \right\rangle_{k=0}}{n_0 \cos\theta} n_1(v)k_1(v) \int_0^\infty e^{-2z/d_p(\theta,v)} dz \qquad (2.13)$$

By substituting Equation 2.6 into Equation 2.13, the following expression is obtained:

$$2\frac{1-R(\theta,v)}{1+R(\theta,v)} = \frac{2\pi v \left\langle E_0^2(\theta,v) \right\rangle_{k=0} n_1(v)k_1(v)d_p(\theta,v)}{n_0 \cos\theta} \qquad (2.14)$$

When absorption is small (*i.e.*, $R(\theta,v)$ is close to unity) the above equation is further simplified to:

$$\ln R(\theta,v) = \frac{2\pi v n_1(v)k_1(v)d_p(\theta,v)\left\langle E_0^2(\theta,v) \right\rangle_{k=0}}{n_0 \cos\theta} \qquad (2.15)$$

$$\mathbf{A}(\theta,v) = \frac{2\pi v n_1(v)k_1(v)d_p(\theta,v)\left\langle E_0^2(\theta,v) \right\rangle_{k=0}}{\ln(10)n_0 \cos\theta} \qquad (2.16)$$

where $\mathbf{A}(\theta,v)$ is the absorbance, which is the value one normally obtained from spectrometer. However, one should not confuse the absorptance $A(\theta,v)$ given in Equation 2.6 and the absorbance $\mathbf{A}(\theta,v)$ given in Equation 2.16 because they are defined from the different criteria.

Equation 2.16 also indicates that spectral intensity is directly related to material characteristic. However, the expression is limited to small absorption since it is derived from the MSEvF. However, the expression is the most convenient form for expressing quantitative relationship between spectral intensity and material characteristic.

2.3.3   Problem of Sample Contact in ATR Measurement

Since ATR FT-IR is a surface sensitive technique, in order to obtain good ATR spectra, a very good contact between the sample and ATR prism or an IRE is required. Liquid samples always have a perfect optical contact with an IRE. Solid samples, on the other hand, rarely have a good contact with an IRE although their surface is obviously flat. This is due to the surface irregularity of the samples, imperfect flatness throughout the surface, defect on the surface. In order to gain a good contact between solid samples and an IRE, the pressure must be applied. If the sample is harder or tougher than the prism material, the applied pressure will lead to the rapid deterioration of the prism and still no optical contact is obtained. Unfortunately, the high refractive index materials used for ATR FT-IR are not very strong and the high frequency regions require a much better contact.

2.4   Novel ATR FT-IR Microscopy

2.4.1   Tranflectance Phenomena

In principle, a faceted diamond was cut in such a proportion that number of internal reflections within the diamond is enhanced. To increase the number of total internal reflection, the cutting proportion of diamond is carefully designed with respect to its reflective index, size and carat weight. The number of total internal reflections depends on the angle and the positions that light enters the diamond. The greater number of reflections within the diamond, the better the fire and brilliance of the faceted diamond [23-24].

To obtain the better understanding of the tranflectance phenomenon under the employed cut proportion of diamond, ray tracing of radiation in diamond are shown in Figure 2.11 [25]. A round brilliant cut diamond consists of 57+1 facets depending on the presence of the culet. Since the refractive index of the diamond ($n_{diamond}$ = 2.417) is greater than air (n_{air} = 1.0) total internal reflection at diamond/air is observed when radiation traveling inside the diamond impinges the interface with the angle of incidence greater than the critical angle. The critical angle, θ_c, is given in term of the refractive indices by $\theta_c = \sin^{-1} (n_{air}/n_{diamond})$ and is equals to 24.44° for diamond/air interface.

A

CROWN

Table Facet
Star Facet
Bezel Facet
Upper Girdle Facet
Girdle
Lower Girdle Facet
Pavilion Facet
Culet

PAVILION

B

Ray	Angle (degree)					
	α_i	β_i	θ_1	θ_2	β_t	α_t
a	4.84	2	43	55	14	35.78
b	0	0	41	57	16	41.77
c	4.84	2	39	59	38	N/A
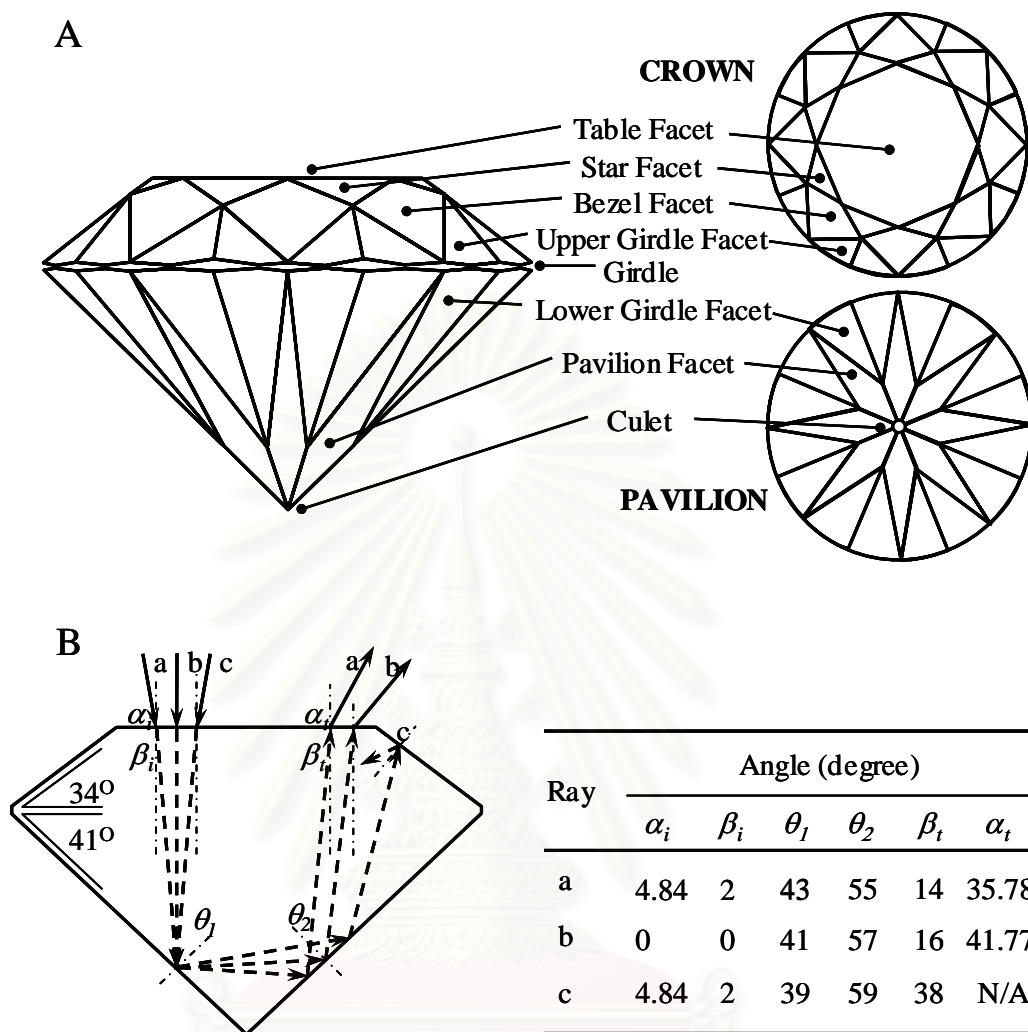
Figure 2.11 A schematic drawing of a round brilliant cut diamond with Tolkowsky's recommended cut proportion (A). Ray tracing of the incident radiations travel within a round brilliant cut diamond (B), and a summary of angles at diamond/air interface.

In order to collect tranflectance infrared spectra of faceted diamond using an infrared microscope, the infrared radiation is coupled into and is collected from the table facet by built-in 15X Cassegrian objective. According the optical design of objective, the coupled infrared radiation is inherently converging [26]. For the coupled infrared radiation with a normal incidence to the table facet, the radiation totally reflects at the pavilion facet. Under the employed cut proportion shown in Figure 2.11B, (*i.e.*, a set of Tolkowsky's recommended cut proportion with pavilion

angle of 41° and crown angle of 34°), the angles of reflection at pavilion facet are 41° and 57° for the first and the second reflections, respectively. The radiation reaches the diamond/air interface at the table facet at 16° angle of incidence and refracts into air with an angle of 41.77°. Due to the complex cut surfaces of the faceted diamond and the divergence of the coupled radiations, the radiations impinge the table facet with different angles and undergo different radiations before emerging into the air. However, some radiations may not emerge from the table facet but undergo multi internal reflections before emerging into air at any other facet.

According to the traveling path of the coupled radiation in Figure 2.11B, the out going radiation from the table facet is defined as the *transflected radiation*. Since diamond has absorption bands in the mid infrared region, attenuations of the infrared radiation at diamond characteristic absorption frequencies are expected. As a result, by collecting the transflected radiation, the absorption spectra of diamond can be measured [25].

2.4.2 Using a Faceted Diamond as an IRE

A novel technique for ATR FT-IR spectral acquisition by infrared microscope with gem quality faceted round brilliant cut diamond as an IRE. The benefits of the diamond are its strength and hardness, its chemical resistance to virtually any materials and it offers optical transparency in mid infrared region. Under the ATR condition, the material was placed against the tip of diamond. Due to the high refractive index of diamond ($n_{diamond} = 2.417$), the evanescent field exponentially decays as a function of depth from the surface of the material with lower refractive index. Therefore, it can be exploited of the physicochemical characterization of material as that in the conventional ATR FT-IR technique [20].

Diamond has three major absorption bands in the mid infrared region, namely one-phonon (1400-900 cm^{-1}), two-phonon (2650-1500 cm^{-1}), and three-phonon (3900-2650 cm^{-1}) absorptions. The absorptions are associated with impurities and defects in diamond crystal structure. The absorption magnitude in the one-phonon region depends strongly on the concentration of nitrogen impurity within the diamond structure. Diamond with high nitrogen content always shows over absorption while that with low nitrogen content does not show significant absorption in this region. Transflectance spectra of round brilliant cut diamonds (*i.e.*, ATR spectra of air) with different magnitude of nitrogen impurities are shown in Figure 2.12. A diamond with low nitrogen content can be employed as an IRE. The two-phonon region is the intrinsic absorption of diamond crystal structure. Although the two-phonon region is always over absorbing, it has little effect on analytical application since most organic materials do not absorb light in this region. The three-phonon region, on the other hand, is very weak. It imposes insignificant interference with the absorption of the materials.
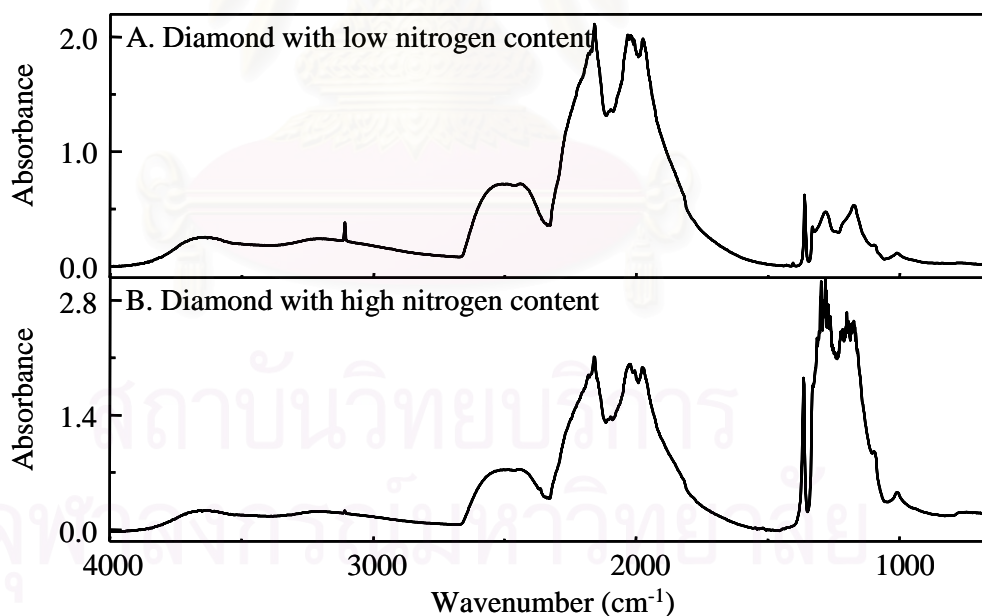
Figure 2.12 Transflectance spectra of a brilliant cut diamond with low nitrogen content (A), and diamond with high nitrogen content (B).

The novel diamond IRE has two configurations: a sharp-tip and a flat-tip. Since diamond is hardest material, a sharp-tip diamond IRE can penetrate into the sample, therefore, bulk information of material was obtained. The surface information of sample was acquired by a flat-tip diamond IRE. Unlike conventional IREs, the novel diamond IRE has a small sampling area. The diamond tip (*i.e.*, the culet and the part of the pavilion) is utilized as sampling area where the evanescent field interacts with the sample. Pressure can be applied onto the sample against the diamond IRE in order to ensure the optimal contact during spectral acquisition. Figure 2.13A and 2.13B show the sample bought into contact with a sharp-tip and a flat-tip diamond IRE, respectively. Due to the small contact area of diamond IRE, the observed tranflectance spectra were not affected by the regularity or roughness of the materials. Moreover, a transflectance spectrum does not suffer from the sample size since the sampling area is controlled by the size of the diamond IRE.
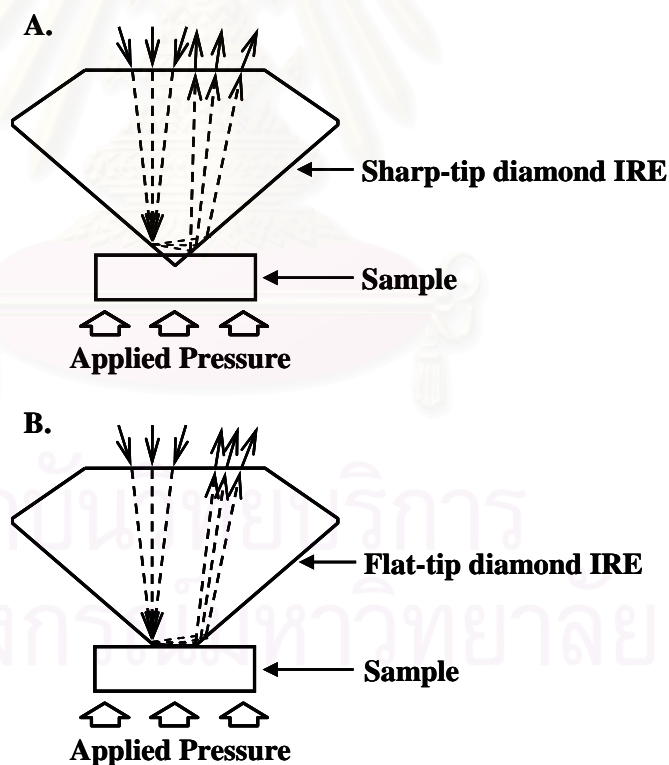
Figure 2.13 The sample brought into contact with a sharp-tip diamond IRE (A), and a flat-tip diamond IRE (B).

Although the diamond IRE has the absorption bands in the mid infrared region, the absorption of diamond can be subtracted from the observed spectra of samples. Unique spectral features of the samples were revealed, shown in Figure 2.14. However, the contribution of the diamond cannot be completely eliminated due to the differences of the optical configurations of the system (*i.e.*, diamond/air and diamond/sample).
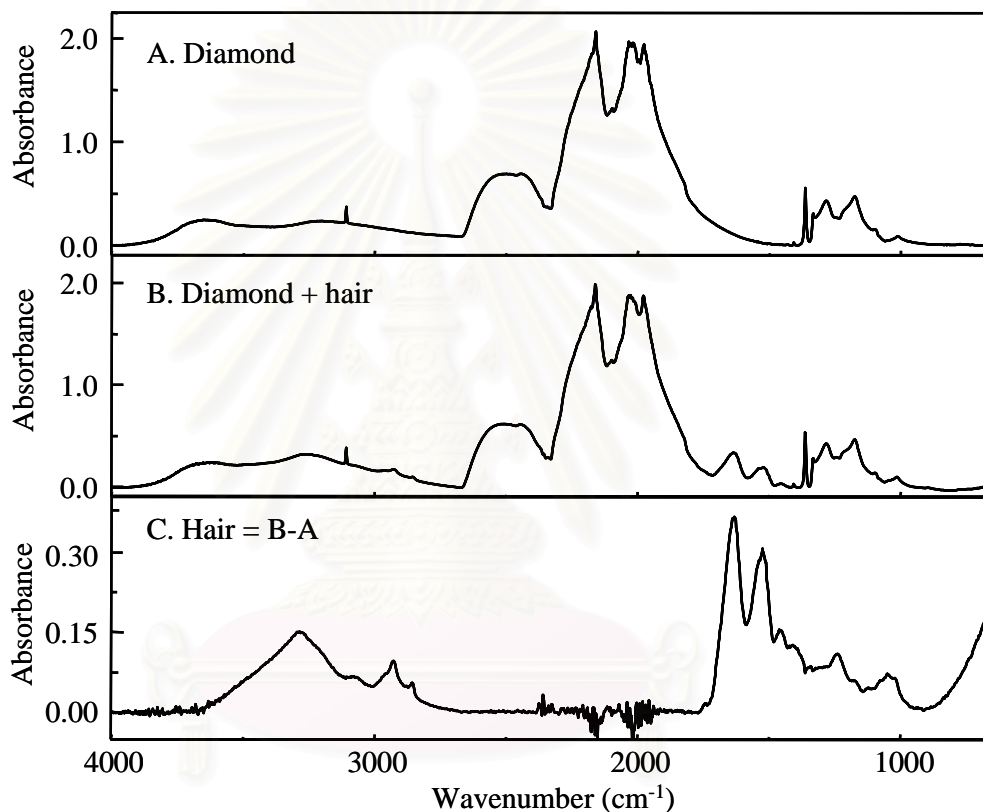
Figure 2.14 ATR spectra of the novel diamond IRE (A), diamond IRE and human hair (B), and human hair acquired by the novel diamond IRE. When the contributions of the diamond IRE were subtracted, the unique spectral features of human hair were revealed (C).

CHAPTER III

EXPERIMENTAL SECTION

The study of single fibers, one of the many applications of attenuated total reflection Fourier transform infrared (ATR FT-IR) microscopy, is widely applied in forensics, the textile and polymer industries. Characterization of single fibers is difficult due to only a small amount of sample is available for study, as occurring in fabric defects or fiber contaminations. Moreover, when it is desirable to preserve the bulk of the textile, as is the case with textiles of historic interesting.

The interest of using natural plant fiber as reinforcing agents in composite materials based on polymeric matrices is presently increasing attention because of the multiple advantages, including cost effective, low density, non-toxicity, high specific properties, no abrasion during processing, and recyclability. Due to the poor wettability and absorbability towards polymers resulting from the highly hydrophilicity of plant fiber, the adhesion between the fibers and polymeric matrices is generally insufficient. The deficiently adhesion leads to a weak load transfer from the matrix to the fibers, which induces a low reinforcing effect. In order to reduce the hydrophilicity of plant fibers and to improve their adhesion properties, it is necessary to undertake a chemical modification of their surface, such as esterification [27], silane treatment [28-32], graft copolymerization [33-34], and treatment with other chemicals [31, 33].

The measured fiber samples were plant fibers (sisal, and jute fiber), animal fibers (silk fibers, and human hairs), and synthetic fibers (thread fibers).

3.1   Materials and Equipments

3.1.1   Equipments for Diamond μATR Sensor

1. Reflection adjustable plate
2. Probing head
3. Gem quality round brilliant cut natural diamonds
   3.1   Sharp-tip diamond 0.0910 carat (type IaB natural diamond)
   3.2   Flat-tip diamond 0.0980 carat (type IaA natural diamond)

3.1.2   Instruments for Data Acquisition

1. Nicolet Magna 750 FT-IR spectrometer equipped with NICPLAN^{TM} infrared microscope
2. Single reflection attenuated total reflection (SATR) accessory (the Seagull^{TM}, Harrick Scientific, USA) with a Ge IRE at the incident angle of 45°

3.1.3   Measured Fiber Samples

1.   Natural fiber
    1.1   Plant fibers
        1.1.1   Sisal fibers
            1.1.1.1   Untreated sisal fibers
            1.1.1.2   Pretreated sisal fibers
                - Sisal fibers extracted by a mixture of methanol and benzene (1:1).
            1.1.1.3   Sisal fibers treated with 2 wt% NaOH aqueous solution
            1.1.1.4   Sisal fibers treated with organosilane coupling agent

      - Sisal fibers treated with 2 wt% octadecyltrimethoxysilane (octadecyl-silane) for 1, 3, 5, and 24 h.

      - Sisal fibers treated with 2 wt% 3-methacryloxypropyltrimethoxysilane (methacrylate silane) for 1, 3, 5, and 24 h.

      - Sisal fibers treated with 2 wt% 3-aminopropyltriethoxysilane (amino-silane) for 1, 3, 5, and 24 h.

1.1.2 Jute fibers

1.1.2.1   Untreated jute fibers

1.1.2.2   Pretreated jute fibers

      - Jute fibers extracted by a mixture of methanol and benzene (1:1).

1.1.2.3   Jute fibers treated with 2 wt% NaOH aqueous solution

1.1.2.4   Jute fibers treated with organosilane coupling agent

      - Jute fibers treated with 2 wt% 3-aminopropyltriethoxysilane (amino-silane) for 1, 3, 5, 7, 10, and 24 h.

1.2 Animal fibers

    1.2.1 Silk fibers

1.2.1.1   Untreated silk fibers

1.2.1.2   Silk fibers treated with a 2 wt% Na_2CO_3 aqueous solution

1.2.1.3   Dyed silk fibers

    1.2.2 Human hairs

2. Synthetic fibers

    2.1 Thread fibers

3.2 Default instrumental Parameters

Nicolet Magna 750 FT-IR Spectrometer

Instrumental Setup

Source	Standard Globar^{TM} Infrared High Source
Detector	Mercury-Cadmium-Telluride (MCT)
Beam splitter	Ge-coated KBr

Acquisition Parameters

Spectral resolution	4 cm^{-1}
Number of coadded scans	256 scans
Spectral format	Absorbance

Advanced Parameters

Zero filling	none
Apodization	Happ-Genzel
Phase correction	Mertz

NICPLAN^{TM} Infrared Microscope

Instrumental Setup

Source	Standard Globar^{TM} Infrared High Source
Detector	Mercury-Cadmium-Telluride (MCT)
Beam splitter	Ge-coated KBr

Acquisition Parameters

Spectral resolution	4 cm^{-1}
Number of coadded scans	256 scans
Spectral format	Absorbance
Aperture size	70

Advanced Parameters

Zero filling	none
Apodization	Happ-Genzel
Phase correction	Mertz

3.3   The homemade diamond μATR sensor

The diamond μATR sensor accessory consists of two major components, the reflection adjustable plate and probing head. The accessory and the infrared microscope were employed for material characterization.

3.3.1   Reflection adjustable plate

Components of the reflection adjustable plate are shown in Figure 3.1. The upper adjustable plate was combined with the lower plate and the three knobs. The three knobs setting on the corner of accessory were employed for adjustment of the reflecting plane perpendicular to the incident infrared beam. The brass ring was mounted into the adjustable plate to support the probing head.

Brass ring

Upper adjustable plate

Three knobs for
focal plane adjustment

Lower plate

Adjustable plate equips
with brass ring

Side view

Top view
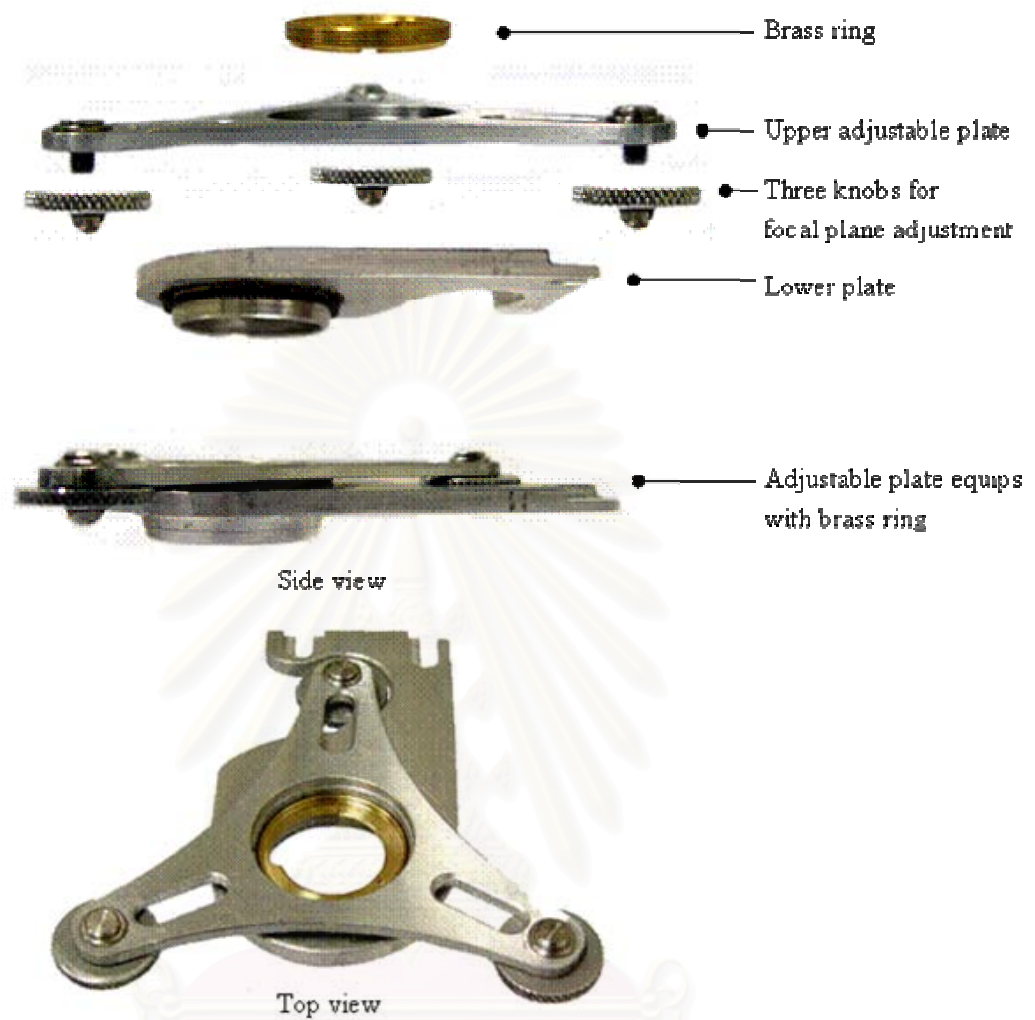
Figure 3.1   Composition of the reflection adjustable plate.

3.3.2 Probing head

The components of the probing head are shown in Figure 3.2. A diamond IRE was placed on the lower diamond holder and held with the upper diamond holder. The sample holder was placed on the pressure applicator in order to apply the sample brought into contact with the diamond IRE. The probing head with a diamond IRE was put into the reflection adjustable plate for the spectral acquisition with infrared microscope. A complete set of homemade diamond µATR sensor are shown in Figure 3.3.

Figure 3.2   Composition of the probing head.

Probing head with
diamond IRE

Adjustable plate

Complete set of homemade
diamond μATR sensor

Side view

Top view
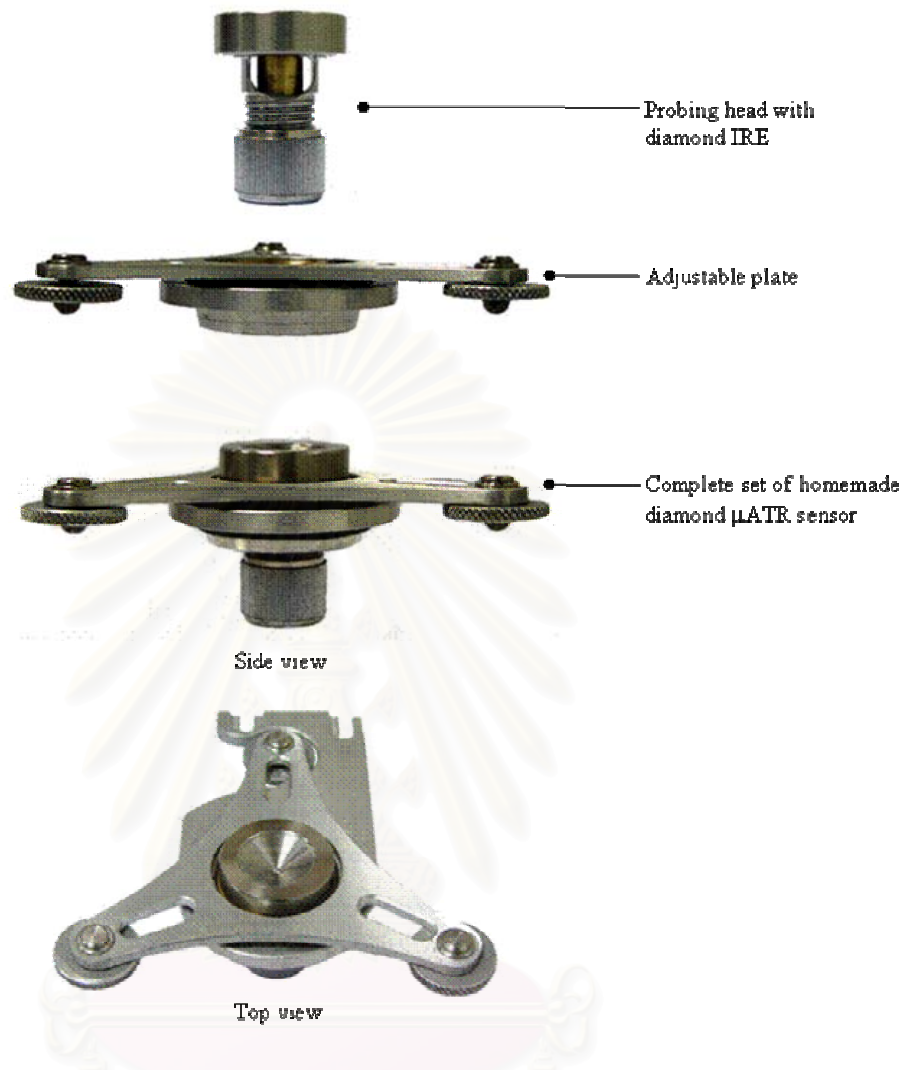
Figure 3.3   Complete set of homemade diamond μATR sensor
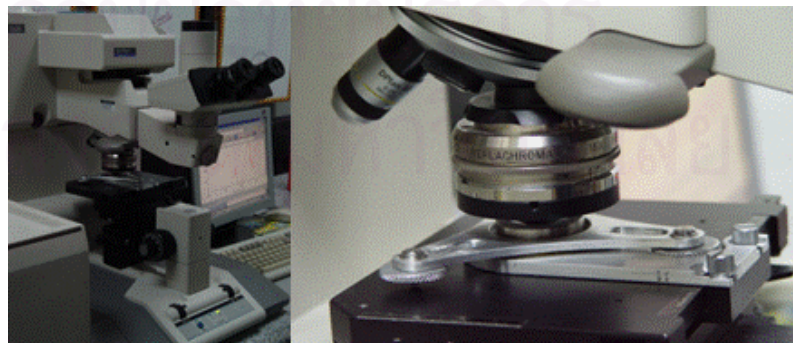
Figure 3.4   Actual experimental setup for homemade diamond μATR sensor with
an infrared microscope.

3.4   Characterization of Single Fibers by ATR FT-IR Spectroscopy

3.4.1   Experimental Procedure for Conventional ATR Measurement

For the conventional ATR experiment, a commercial ATR accessory (the Seagull^{TM}, Harrick Scientific, USA) was employed for spectral acquisition. The Seagull^{TM} was placed in the compartment of the spectrometer. A hemispherical Ge prism was used as an internal reflection element (IRE). Since the angle of incidence in the ATR experiment must be greater than the critical angle, the infrared radiation was coupled through the IRE at the angle of 45°. The spectrum obtained by the Ge IRE without sample was employed as a background for all acquired ATR FT-IR spectra. To collect a spectrum of fiber, a single fiber was placed against the bottom surface of the Ge IRE. The pressure is applied onto the sample in order to ensure an optical contact between the sample and the IRE. ATR spectra of the single fiber were then collected. The same procedure was repeated for all other fibers.
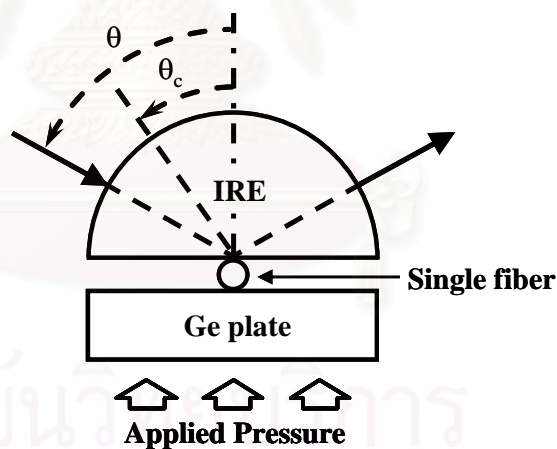
Figure 3.5   Experimental procedure for ensuring the optical contact between a sample and the IRE.

3.4.2 Experimental Procedure for Spectral Acquisition with Diamond μATR Sensor

All ATR FT-IR spectral acquisition were performed on a NICPLAN^{TM} infrared microscope equipped with an MCT detector. Gem quality round brilliant cut natural diamonds were employed as IREs. The diamond IRE has two configurations: a sharp-tip and a flat-tip. The diamond μATR sensor has two major components. First, the reflection adjustable plate placed on the stage of infrared microscope (Figure 3.4). It was employed for adjusting the table facet of the diamond IRE perpendicular to the incoming infrared beam. This operation is performed in order to achieve the maximum energy throughput.

Another part is the probing head to hold a sharp-tip diamond IRE. A single fiber was placed against the tip of diamond and then the pressure was applied. The probing head with a diamond IRE was put into the reflection plane adjustment. Reflection with normal incidence from the table facet of the diamond was employed as a background for all ATR FT-IR spectra acquired by the microscope. An infrared radiation from the infrared microscope via the built-in 15x Cassegrainian objective was coupled into pavilion facet of diamond through the table facet and the transflected radiation was collected. The spectrum of diamond without sample was acquired and was employed for subtracting the diamond spectrum from the observed spectrum of samples. The same procedure was repeated using other fiber samples and the flat-tip diamond IRE. Experimental procedure for spectral acquisition using diamond IRE is shown in Figure 3.6.
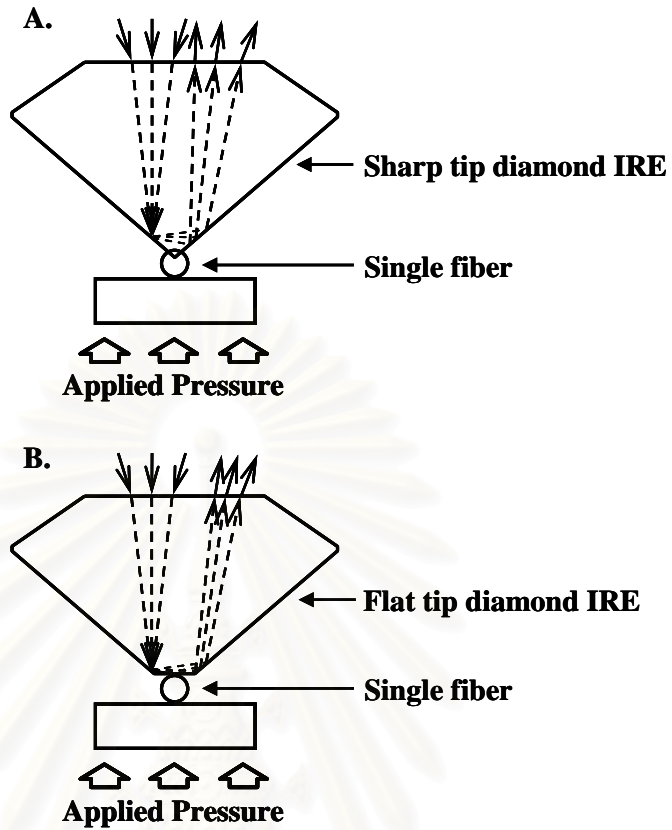
Figure 3.6 Experimental procedure for spectral acquisition using diamond IRE.

CHAPTER IV

RESULTS AND DISCUSSION

4.1 Transflectance Spectra of Diamond IREs

The transflectance spectra of sharp-tip and flat-tip diamond IREs are shown in Figure 4.1. The three principle absorption bands of diamonds (*i.e.*, the three-phonon absorption at 3900-2650 cm^{-1}, the two-phonon absorption at 2650-1500 cm^{-1}, and the one-phonon absorption at 1400-900 cm^{-1}) are clearly observed. The absorption bands in one-phonon region were associated with nitrogen impurities and defects in the diamond crystal structure. Absorption magnitude in this region depends on the nitrogen impurity in the diamond crystal structure. Although the transflectance spectra of two diamond IREs clearly reveal the characteristic bands of the diamond, the absorption bands in one-phonon are different due to the different concentration of nitrogen impurities. Diamond with high nitrogen content always shows the over absorption in this region.
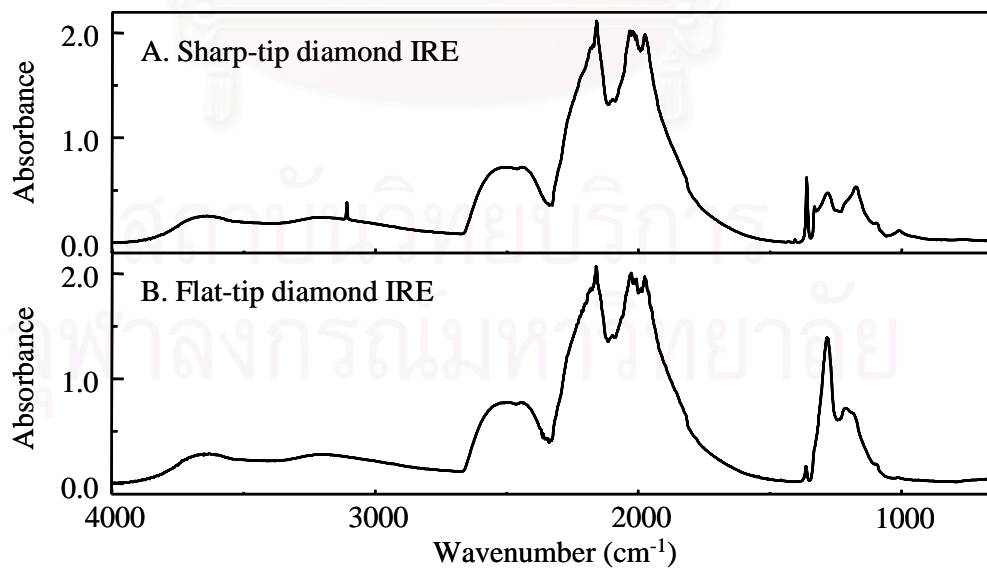
Figure 4.1 Transflectance spectra of two diamond IREs: sharp-tip diamond IRE (A), flat-tip diamond IRE (B).

4.2 Characterization of Single Fiber by ATR FT-IR Spectroscopy

The characterization of single fiber is the significant aspect of the forensic analysis, textile industrial analysis, and polymer industrial analysis. In this work, the novel diamond µATR sensor was used for characterization of natural and synthetic single fibers. The observed spectra acquired by the diamond µATR sensor were compared with those obtained by the conventional ATR.

4.2.1 Natural fiber

The natural fiber was classified into two types: plant fiber and animal fiber. In general, surface modifications include: methanol/benzene dewax treatment, alkali treatment, and silane treatments were applied onto the fibers in order to improve the surface properties of plant fibers (*i.e.*, sisal fiber, and jute fiber). For the animal fibers, silk fibers were treated with alkali solution and dyes while human hairs were treated with shampoo and conditioning cream.

4.2.1.1 Sisal fibers

Sisal fiber consists of mainly cellulose, hemicellulose, lignin, and other minor components. The ATR spectrum of untreated sisal fiber obtained by sharp-tip diamond µATR sensor is illustrated in Figure 4.2a. The band at 1732 cm^{-1} can be assigned as C=O stretching vibration of carboxyl and acetyl groups of hemicelluloses. The bands at 1602 and 1506 cm^{-1} were attributed to the C=C in-plane aromatic stretching vibration from lignin while the band at 1100 cm^{-1} related to asymmetric C-O-C stretching vibration from polysaccharide components [10, 35]. The summary of the band assignments for cellulosic fiber is presented in Table 4.1.

The main purpose of washing sisal fibers with a mixture solution of methanol and benzene is to remove waxes. By comparison between untreated and pretreated sisal fiber in Figure 4.2a and 4.2b, both spectra show the same spectral feature. Although the untreated sisal fiber has the impurity such as waxes, the quantity of this impurity is too small to show up the significant changes in the spectrum of pretreated

sisal fiber. The treatment of the fibers with alkali solution promotes the partial removal of the hemicelluloses, waxes, and lignin present on the surface of the fiber. The spectrum of alkali-treated sisal fiber obtained by the sharp-tip diamond μATR sensor is shown in Figure 4.2c. In general, hemicellulose contains groups absorbing in the carbonyl region which can be soluble in aqueous alkali solutions. It clearly reveals that the band around 1732 cm^{-1} disappears when the fiber is treated by aqueous NaOH solution as shown in Figure 4.2c. It is appreciated that the strong absorption band at 1242 cm^{-1} which is a characteristic of C-OH out-of-plane bending vibration disappears while two new bands appear at 1236 and 1205 cm^{-1} [29-30]. The observed spectra acquired by the sharp-tip diamond μATR sensor were similar to that acquired by the flat-tip diamond μATR sensor (Figure 4.3), and the conventional ATR with Ge IRE (Figure 4.4). The untreated sisal fiber and alkali-treated sisal fiber can be distinguished using ATR technique. As a result, the novel diamond IREs show great potential for characterization of the single fibers.
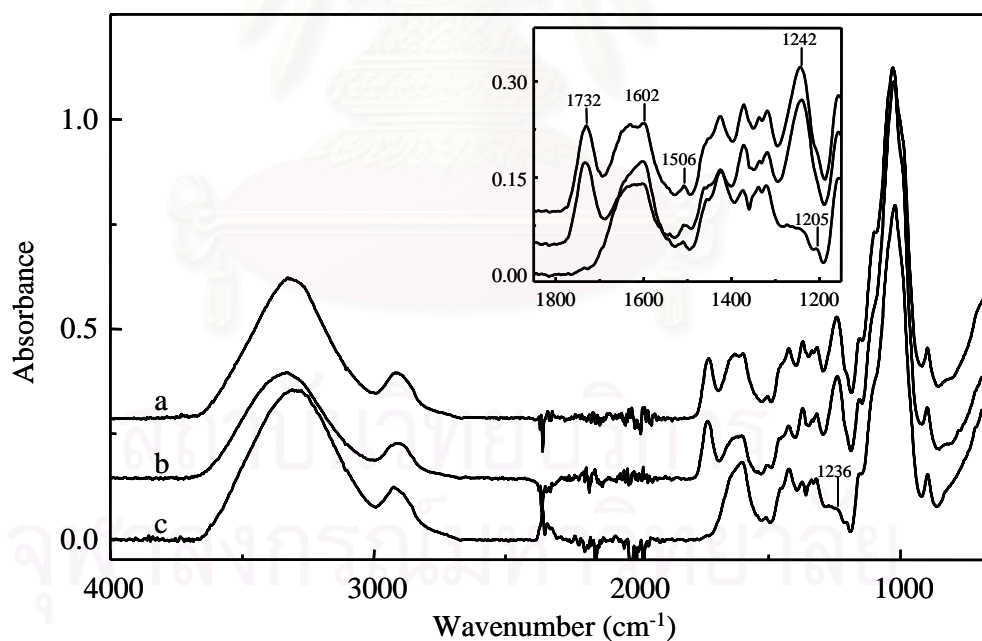
Figure 4.2   ATR spectra of untreated sisal fiber (a), pretreated sisal fiber (b), and alkali-treated sisal fiber (c), acquired by the sharp-tip diamond μATR sensor.
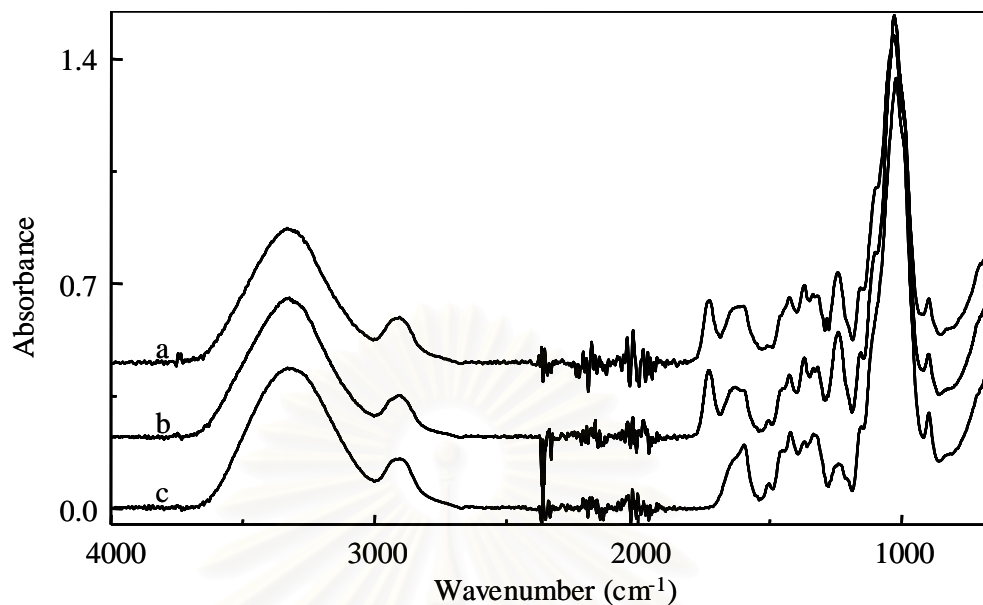
Figure 4.3   ATR spectra of untreated sisal fiber (a), pretreated sisal fiber (b), and alkali-treated sisal fiber (c), acquired by the flat-tip diamond μATR sensor.
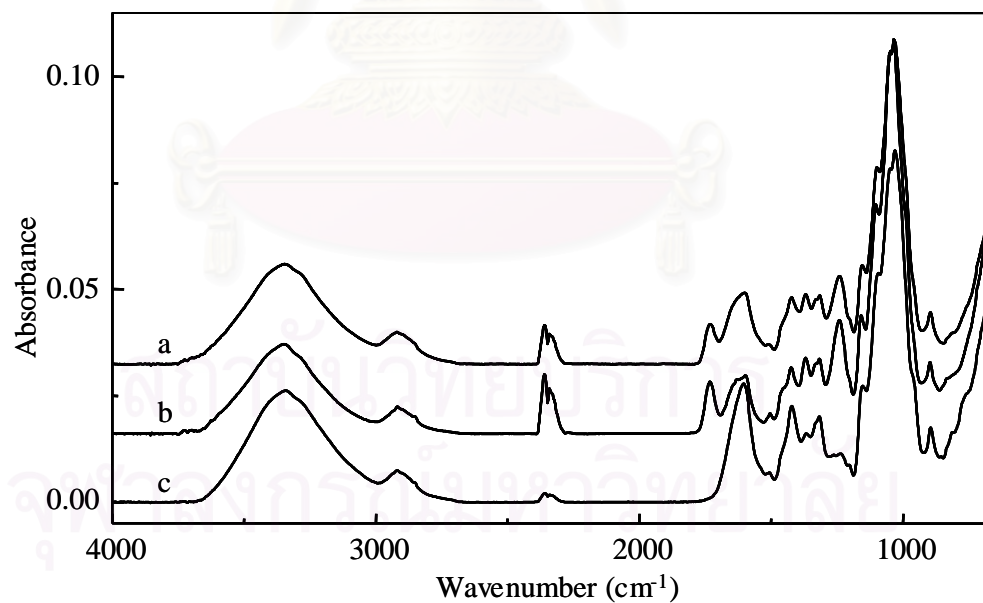
Figure 4.4   ATR spectra of untreated sisal fiber (a), pretreated sisal fiber (b), and alkali-treated sisal fiber (c), acquired by the conventional ATR with Ge IRE.

The ATR spectra of untreated sisal fiber obtained by employing the two configurations of the novel diamond IREs (*i.e.*, sharp-tip and flat-tip diamond IREs) and Ge IRE are shown in Figure 4.5. The observed spectra acquired by the sharp-tip and the flat-tip diamond µATR sensor show the same spectral features as that acquired by the conventional ATR with Ge IRE. In addition, the spectral intensity that observed by the diamond IRE was 10-folds of that of the conventional ATR. Unfortunately, the observed spectra of untreated sisal fibers that acquired by the flat-tip diamond IRE are noticed the interference absorption band of diamond at 1285 cm^{-1}. This result demonstrates that the absorption of diamond in one-phonon region is still presented in subtracted spectra.

Due to the hardness of diamond, the diamond IRE can be applied with the high pressure, thus the technique can eliminate the problems associated with the contact between the IRE and the sample. When considering ATR spectral acquisition with conventional ATR IRE, the energy loss of the reflected radiation at the interface of the IRE and fiber was occurred because the diameter of sampling area of Ge IRE (5 mm) is larger than the size of fiber (< 100 µm). This problem can be resolved by using the sharp-tip diamond IRE. Unlike the conventional IRE and flat-tip diamond IRE, transflectance phenomena from the sharp-tip diamond IRE presents as double reflections at the pavilion facet of diamond. The double reflections can improve the signal-to-noise ratio of the acquired spectrum. Moreover, the distance where the evanescent field decays from the interface of diamond/fiber is greater than the interface of Ge/fiber (angle of incident equal 45° at 1000 cm^{-1}, n_{fiber} = 1.5, $n_{diamond}$ = 2.417, d_p = 1.94 µm, n_{Ge} = 4.0, d_p = 0.66 µm). From these reasons, the spectral intensity that obtained from the diamond IREs were greater than that from the conventional IRE.
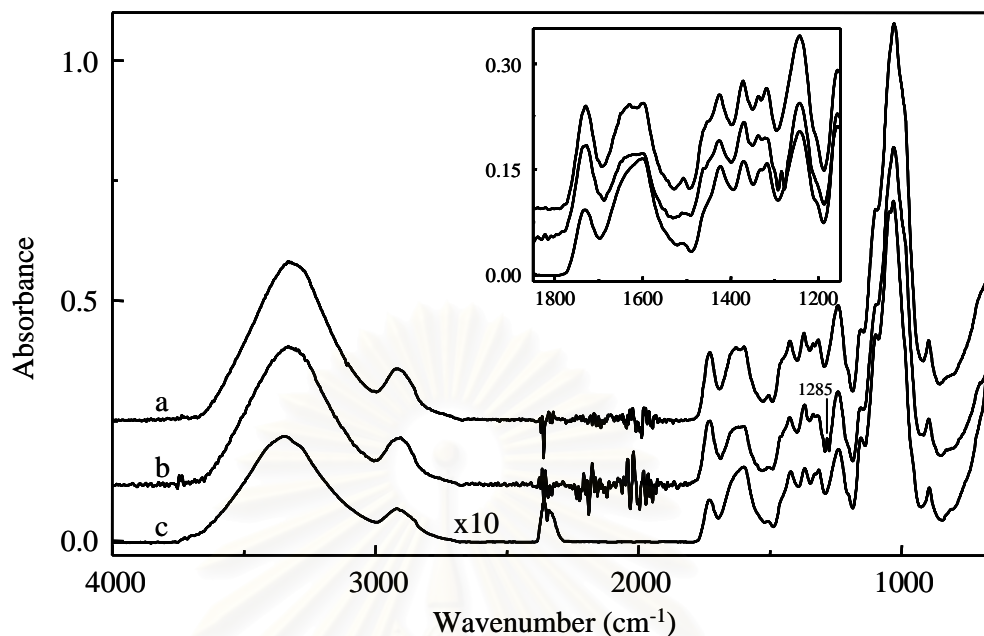
Figure 4.5 ATR spectra of untreated sisal fiber obtained by the sharp-tip diamond µATR sensor (a), flat-tip diamond µATR sensor (b), and conventional ATR (c).

4.2.1.1.1 Octadecylsilane-treated sisal fibers

The spectra of the sisal fibers treated with octadecyltrimethoxysilane acquired by the sharp-tip diamond µATR sensor are shown in Figure 4.6A. The two strong absortion bands at 2919 and 2850 cm^{-1} are the characteristics of the asymmetric and symmetric stretching vibrations of the CH_2 groups of octadecylsilane, respectively. In addition, the absorption bands at 1204 and 1160 cm^{-1} associated with the Si-O-C bond and Si-O-Si bond can be noticed.

Figure 4.6   ATR spectra of alkali-treated sisal fiber and ATR spectra of octadecylsilane-treated sisal fiber with different treatment periods (*i.e.*, 1, 3, 5, and 24 h). The spectra were acquired by the sharp-tip diamond μATR sensor (A) and the conventional ATR (B).

The ATR spectra of octadecylsilane-treated fiber acquired by the conventional ATR are shown in Figure 4.6B. The characteristic of the asymmetric and symmetric stretching vibrations of the CH_2 groups were observed. An absorption band at 1204 cm^{-1} is assigned to the vibration mode of the Si-O-C bond while the absorption bands around 1161, 1055, and 1036 cm^{-1} are assigned to the stretching vibration of the Si-O-Si bond.

The characteristic absorption bands of Si-O-Si at 1161, 1055, and 1036 cm^{-1} confirm the presence of polysiloxanes. The band 1204 cm^{-1}, which is the characteristic of the Si-O-C bond support the condensation reaction between the octadecylsilane and the cellulose on the sisal fiber [8, 29].

Since the sharp-tip diamond IRE can penetrate into the fiber, molecular information of at a greater depth can be collected. The obtained information is the average information coming from the surface and a greater depth of the sisal fiber. Since the characteristic of the cellulosic fiber in region 1170-930 cm^{-1} was very intense, the absorption bands of octadecylsilane-treated sisal fiber at 1055 and 1036 cm^{-1} could not be observed. However, ATR spectra of the sharp-tip diamond μATR sensor can confirm the reaction between the silane coupling agent and the fiber from the characteristic of the stretching vibrations of the CH_2 groups of octadecylsilane and absorption band at 1204 cm^{-1} that associated to the Si-O-C bond. The characteristic absorption band at 1161 cm^{-1} attributed to the presence of the stretching vibration of the Si-O-Si bond can be observed.

The ATR spectra obtained by the sharp-tip diamond IRE and conventional IRE show the different feature of the alkali-treated sisal fiber and octadecylsilane-treated sisal fiber. The spectra of octadecylsilane-treated sisal fiber show that the silane functional group appended to the fiber surface.

4.2.1.1.2 Methacrylate silane-treated sisal fibers

The ATR spectra of with 3-methacryloxypropyltrimethoxysilane-treated sisal fibers obtained by the sharp-tip diamond μATR sensor are illustrated in Figure 4.7A. The band at 1735 cm^{-1} corresponding to C=O stretching vibration of the methacrylate silane. The absorption band at 1159 cm^{-1} is assigned to the stretching of the Si-O-Si bond. An absorption band at 1204 cm^{-1} is associated to the Si-O-C stretching vibration. A slightly increasing of the broad band around 1170-940 cm^{-1} in methacrylate silane-treated sisal fiber can be observed.

The ATR spectra of methacrylate silane-treated sisal fiber acquiring via conventional ATR technique are shown in Figure 4.7B. The band at 1736 cm^{-1} corresponding to C=O stretching vibration was clearly observed. The absorption bands at 1161, 1055, and 1035 cm^{-1} are attributed to the presence of the stretching vibration of the Si-O-Si bond. The former bond is the indicator of the existence of polysiloxanes deposited on the sisal fibers. The characteristic of Si-O-C bond at 1204 cm^{-1} can demonstrate the occurrence of a condensation reaction between the methacrylate silane and the fiber, as discussed above for octadecylsilane-treated sisal fiber [8, 29].
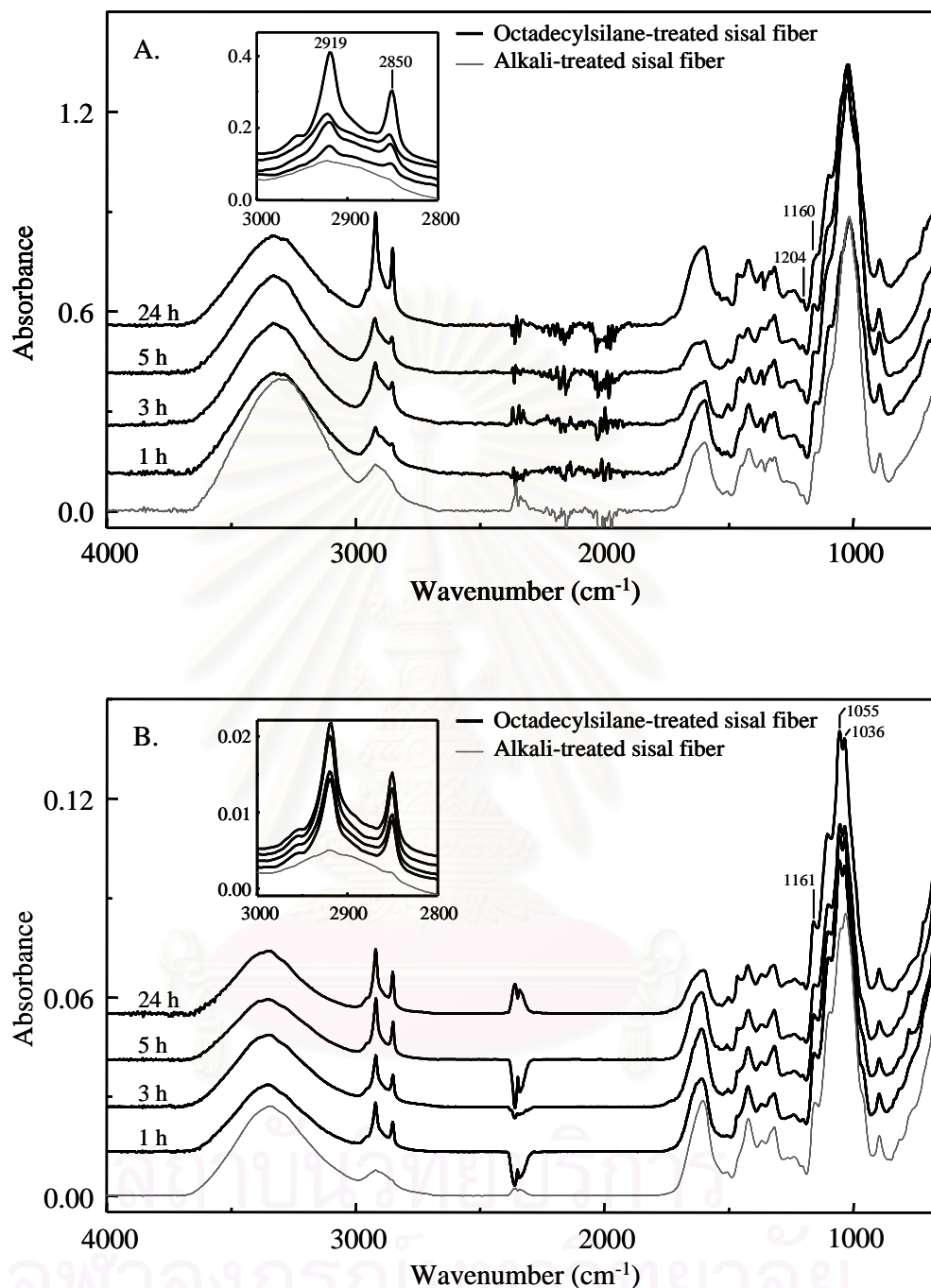
Figure 4.7 ATR spectra of alkali-treated sisal fiber and ATR spectra of methacrylate silane-treated sisal fiber with different treatment periods (*i.e.*, 1, 3, 5, and 24 h). The spectra were acquired by the sharp-tip diamond μATR sensor (A) and the conventional ATR (B).

4.2.1.1.3 Aminosilane-treated sisal fibers

The ATR spectra of 3-aminopropyltriethoxysilane-treated sisal fibers acquired by the sharp-tip diamond μATR sensor are shown in Figure 4.8A. The band at 1599 cm^{-1} is the typical of the deformation mode of NH_2 groups hydrogen bonded to the OH functions of both silanol moieties and cellulosic fiber. The absorption band at 1204 cm^{-1} is associated to the Si-O-C bond. The absorption band at 1159 cm^{-1} is related to the stretching vibration of the Si-O-Si bond. A slight increment of the broad absorption band between 1170-940 cm^{-1} in amino-treated sisal fiber can be observed.

The ATR spectra of aminosilane-treated sisal fiber obtained by the conventional ATR are shown in Figure 4.8B. The band at 1596 cm^{-1} is typical for the deformation mode of NH_2 groups hydrogen bonded to the OH functions of both silanol moieties and cellulosic fiber. The band at 1204 cm^{-1} is the characteristic of Si-O-C bond. This appearance suggested that the sisal fiber was treated with aminosilane by the condensation reaction. The absorption bands at 1161, 1055, and 1035 cm^{-1} are assigned to the stretching vibration of the Si-O-Si bond. From these results, it is seen that the silane was effectively deposited on the fiber surface [8, 29].

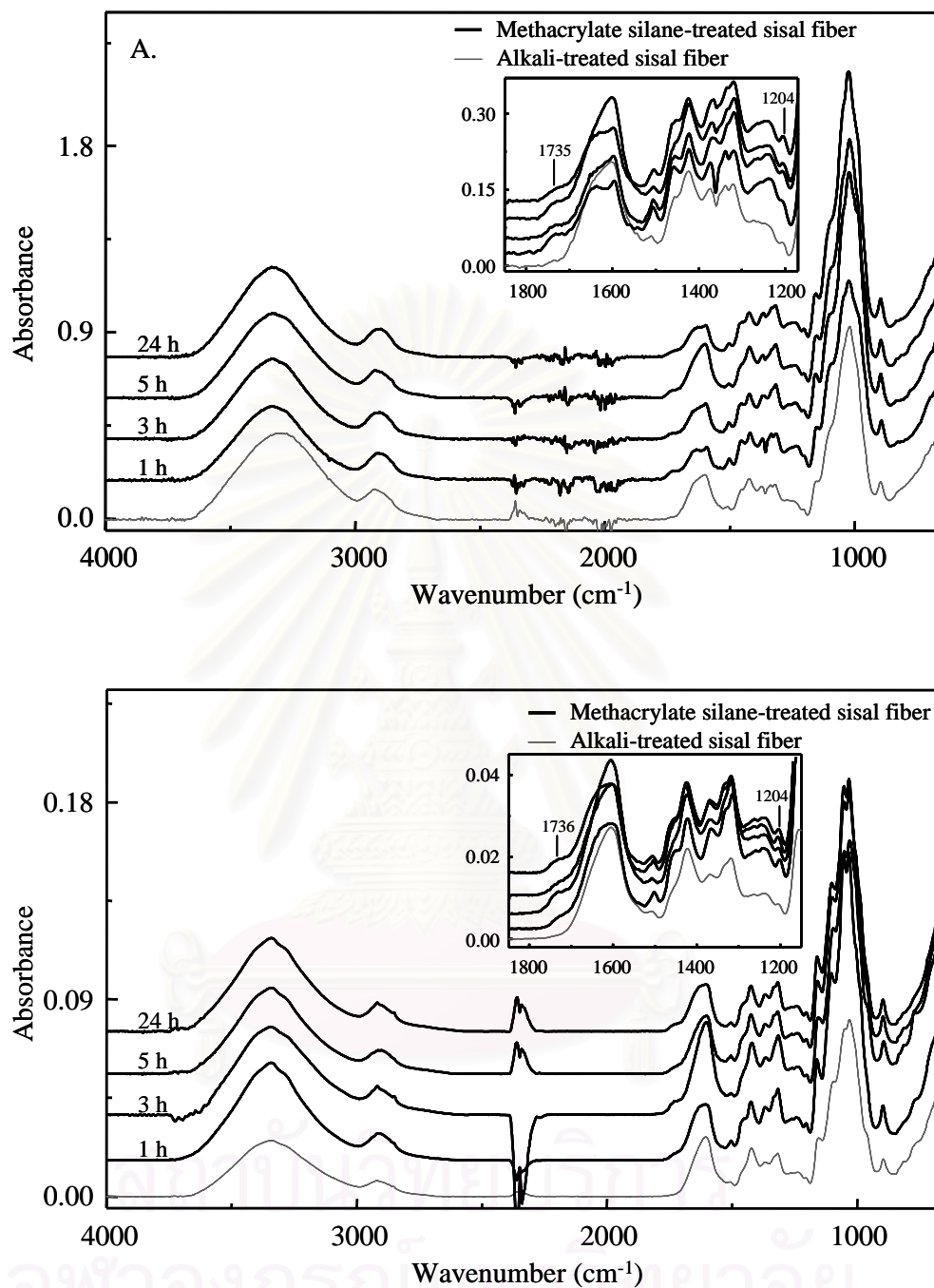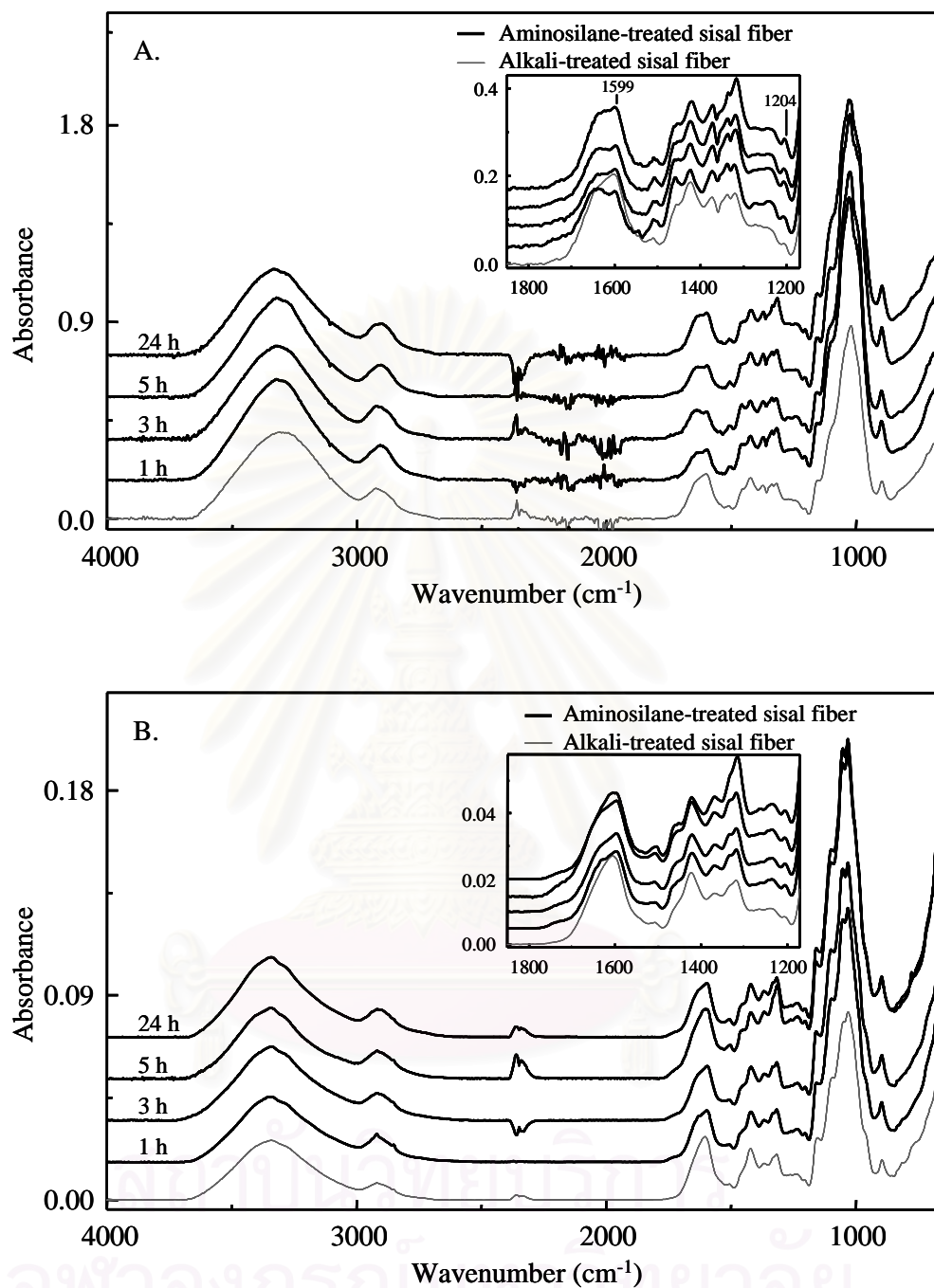**Figure 4.8**   ATR spectra of alkali-treated sisal fiber and ATR spectra of aminosilane-treated with different treatment periods (*i.e.*, 1, 3, 5, and 24 h). The spectra were acquired by the sharp-tip diamond µATR sensor (A) and the conventional ATR (B).

The single fibers can be characterized by using the diamond μATR sensor and the conventional ATR. The observed spectra show the presence of Si-O-C and Si-O-Si bonds on the surface of sisal fiber which suggest the reaction between aminosilane and the fiber.

As a result, all of the observed spectra demonstrated that the sharp-tip diamond μATR sensor is useful for single fiber characterization. The untreated sisal fiber, alkali-treated sisal fiber, octadecylsilane-treated sisal fiber, methacrylate silane-treated sisal fiber, and aminosilane-treated sisal fiber can be distinguished via ATR spectra of diamond μATR technique. A summary of band assignments for silane-treated cellulosic fiber is shown in Table 4.2.

4.2.1.2 Jute fibers

Jute fiber principally consists of mainly cellulose, hemicellulose, lignin, and other minor organic materials. The ATR spectrum of untreated sisal fiber acquired by the sharp-tip diamond μATR sensor is shown in Figure 4.9A(a). A broad absorption band in the region 3330 cm^{-1} which is the characteristic of hydrogen bonded O-H stretching vibration can be observed in all spectra. The strong absorption band at 1732 cm^{-1} is associated to C=O stretching vibration of carboxyl and acetyl groups of hemicellulose. The observed spectra of the C=C in-plane aromatic stretching vibration at 1596 cm^{-1} and 1506 cm^{-1} can imply unsaturation of jute fiber from lignin. The band at 1103 cm^{-1} (glycosidic ether band) is assigned as asymmetric C-O-C stretching vibration from polysaccharide components. The observed spectra of untreated jute fiber acquired by the sharp-tip diamond μATR sensor show the same spectral features as that acquired by the conventional ATR with Ge IRE (Figure 4.9B).

The jute fibers were pretreated with mixture solution of methanol and benzene for removing waxes. The pretreated jute fiber has no significantly changes in spectral feature as shown in Figure 4.9A(b). The main effect of washing jute fiber with an aqueous alkali solution is to remove the waxes, hemicelluloses, and a partial

removing of the lignin inherent on the surface of fiber. The spectrum of alkali-treated sisal fiber acquiring via diamond μATR technique is shown in Fig. 4.9A(c). It is noted that the band around 1732 cm^{-1} in the pretreated jute fiber is no longer existed in alkali-treated jute fiber. The strong band at 1240 cm^{-1} is the characteristic of C-OH out-of-plane bending vibration disappears while the prominent two bands at 1238 and 1206 cm^{-1} appear [29-30]. The observed spectra acquired by the sharp-tip diamond μATR sensor were similar to that acquired by the conventional ATR with Ge IRE.

The observed spectra show the different spectral features between the untreated jute fiber and alkali-treated jute fiber, thus they can be distinguished by the diamond μATR sensor and the conventional ATR technique.
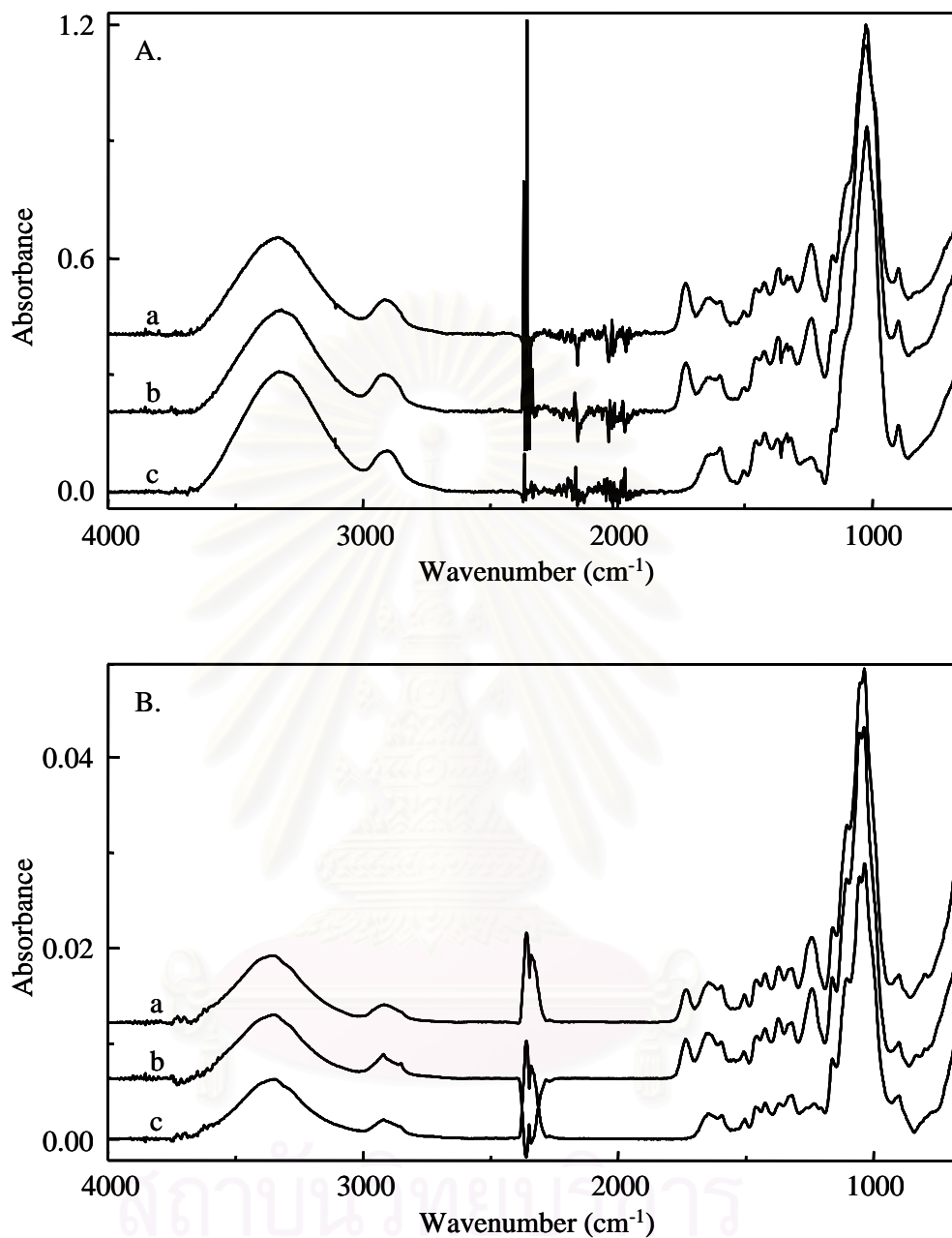
Figure 4.9 ATR spectra of untreated jute fiber (a), pretreated jute fiber (b), and alkali-treated jute fiber (c). The spectra were acquired by the sharp-tip diamond µATR sensor (A) and the conventional ATR (B).

4.2.1.2.1 Aminosilane-treated jute fibers

The spectra of the jute fibers treated with 3-aminopropyltriethoxysilane obtained by sharp-tip diamond µATR sensor are shown in Figure 4.10A. The absorption band at 1207 cm^{-1} is related to the Si-O-C bond.

The ATR spectra of aminosilane-treated jute fiber acquired by the conventional ATR with Ge IRE are shown in Figure 4.10B. The absorption band at 1204 cm^{-1} is the characteristic of Si-O-C bond. The bands at 1162, 1056, and 1035 cm^{-1} are associated to the stretching vibration of the Si-O-Si bond. Unlike the spectra of aminosilane-treated sisal fiber, the absorption of deformation mode of NH$_2$ groups could not be noticed in both the observed spectra from sharp-tip diamond µATR sensor and the conventional ATR technique. It can be suggested that the reaction between aminosilane and the jute fiber was not affected by the treatment process.
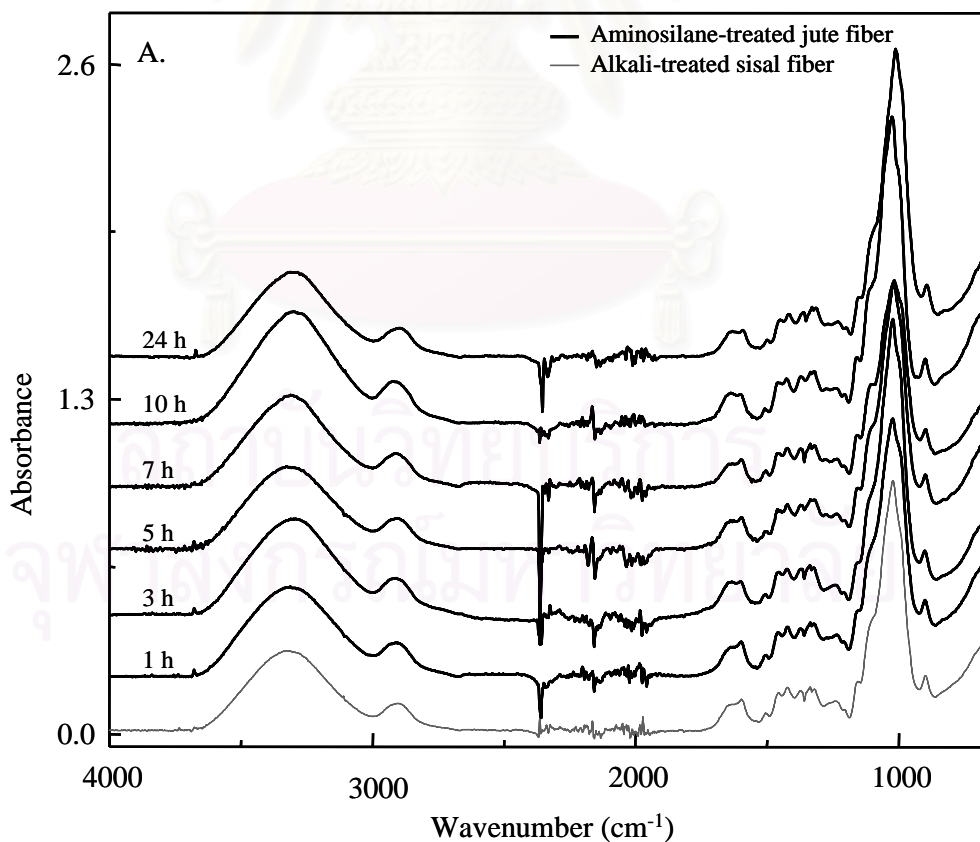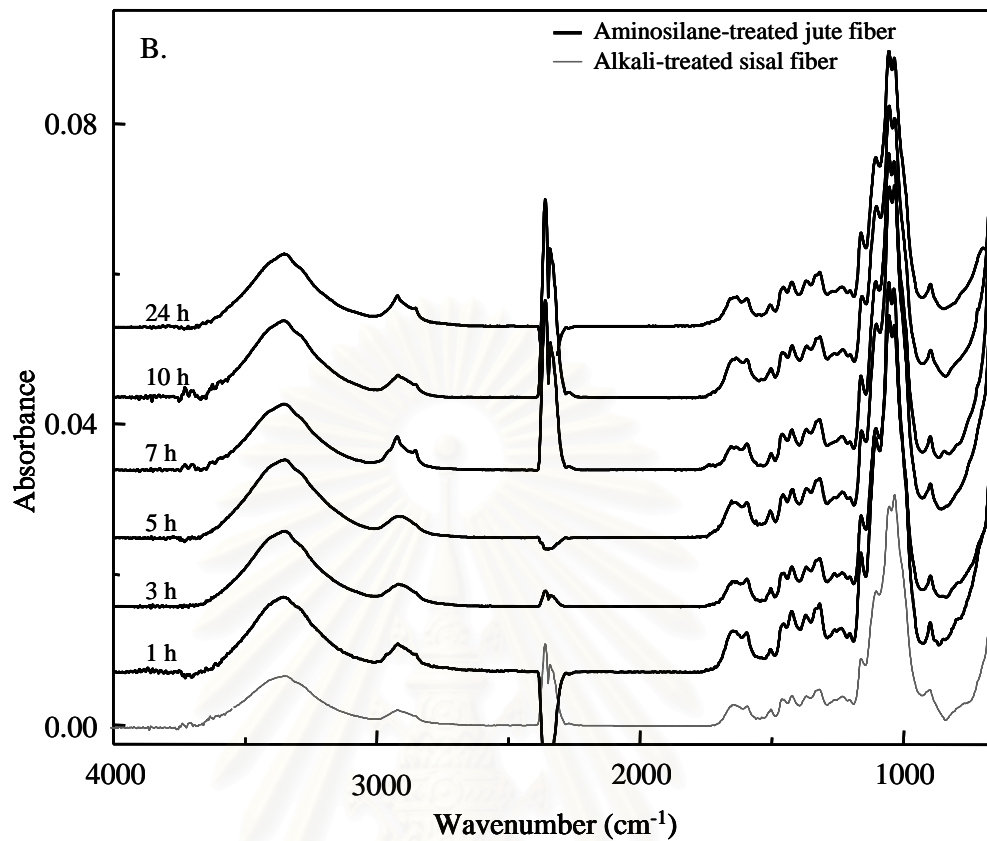
Figure 4.10 ATR spectra of alkali-treated sisal fiber and ATR spectra of jute fiber treated with aminosilane with different treatment periods (*i.e.*, 1, 3, 5, 7, 10, and 24 h). The spectra were acquired by the sharp-tip diamond µATR sensor (A) and the conventional ATR (B).

Table 4.1

Peak assignments corresponding ATR spectra for cellulosic fiber

Wavenumber (cm^{-1})		Assignments
diamond µATR sensor	conventional ATR	
3330	3340	H-bonded of OH stretching
~2900	~2900	C-H stretching
1732	1732	C=O stretching
1602	1600	C=C in-plane aromatic stretching
1506	1504	C=C in-plane aromatic stretching
1458	1458	C-H bending, C-OH 1° & 2° alc. bending
1425	1425	C-H bending
1371	1370	C-H bending
1318	1318	C-H bending
1242	1242	C-OH out-of plane bending
1158	1158	Asym. C-C ring breathing, stretching
1100	1102	Asym. C-O-C stretching
1028	1032	C-O stretching
898	897	Sym. C-O-C in-plane stretching

Table 4.2

Peak assignments corresponding ATR spectra for silane-treated cellulosic fiber

Wavenumber (cm^{-1})		Assignments
diamond μATR sensor	conventional ATR	
2919	2919	Asym. C-H stretching of CH$_2$
2850	2850	Sym. C-H stretching of CH$_2$
1735	1736	C=O stretching
1599	1596	N-H bending of NH$_2$, H-bonded of cellulosic fiber
1205	1204	Asym. Si-O-C stretching
1160	1161	Si-O-Si stretching
-	1055	Si-O-Si stretching
-	1036	Si-O-Si stretching

4.2.1.3 Human hairs

The main component of human hair is keratin proteins, water, lipid, pigment, and trace elements. In this study, the human hairs from Asian females without color treatment were investigated. The hairs were cleaned with shampoo and then washed with water. Figure 4.11A shows the cleaned-human hair acquired by the sharp-tip diamond μATR sensor. The observed spectra show a broad band at 3280 cm^{-1} attributable to O-H stretching vibration of water together with N-H stretching vibration. The predominant absorption bands at 1636 and 1520 cm^{-1} related to amide (I) and amide (II) vibrations, respectively.

The C=O stretching vibration and a small contribution from N-H bending vibration correspond to vibrational mode of Amide I while C-N stretching vibration together with N-H in-plane bending vibration as that of amide II. The absorption band around 1330-1200 cm^{-1} attributed to amide III vibrational mode which is N-H

in-plane bending vibration plus C-N stretching vibration and O=C-N bending. The absorption band at 1453 cm^{-1} is the CH deformation. The bands at 1121, 1075, and 1046 cm^{-1} due to the absorption of SO_2, SO, and S=O, respectively [36-38]. A summary of the ATR spectral assignments of human hair is presented in Table 4.3.

In order to ensure the sensitivity of the diamond μATR technique, the ATR spectrum of the cleaned-human hairs with shampoo and water was compared to that cleaned with shampoo and carefully washed with water several times. The typical results are shown in Figure 4.11A. The former spectrum shows absorption band at 1048 and 1023 cm^{-1} while these bands cannot be observed in the latter spectrum. By comparison, the identical samples were also investigated by conventional ATR. As shown in Figure 4.11B, the obtained spectrum of the human hairs cleaned with shampoo and water shows the absorption bands at 1045 and 1018 cm^{-1}. It is noted that these peak positions of the same human hairs are slightly different from that acquired by diamond μATR sensor. This is due to the sharp-tip diamond IRE can penetrate into the hair, molecular information at a greater depth can be collected. The obtained information is the average information coming from the surface and a greater depth of the hair. The peak positions of human hair cleaned with shampoo acquired by the sharp-tip diamond μATR sensor were slightly shifted from that acquired by conventional ATR. The absorption band at 1018 cm^{-1} is the characteristic of Si-O-Si stretching vibration of silicone oil in the shampoo. The increment of the bands between 1135-750 cm^{-1} is attributed to the overlapping absorption band of the hair and shampoo.
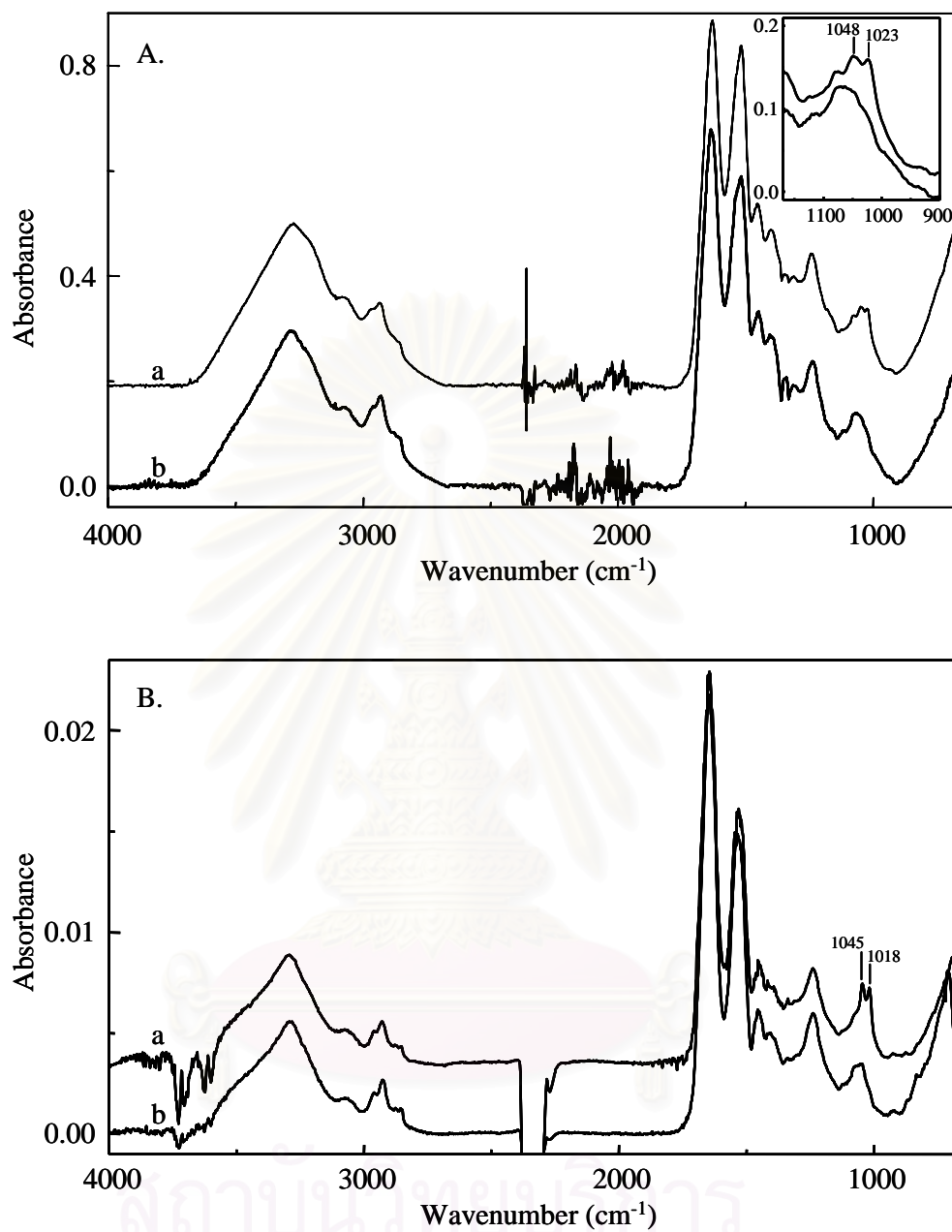
Figure 4.11 ATR spectra of hair cleaned with shampoo and washed with water (a), and hair cleaned with shampoo and washed with water several times (b). The spectra were acquired by the sharp-tip diamond μATR sensor (A) and the conventional ATR (B).

To ensure that the silicone oil was present in shampoo and conditioning cream, the single human hair coated with conditioning cream was placed against the bottom surface of the Ge IRE and the spectrum was observed as shown in Figure 4.12a. When removing the hair out off the IRE, the spectrum was then observed as shown in Figure 4.12b. Regarding the obtained spectrum of the hair, the strong absorption band of Si-O-Si stretching vibration at 1016 cm^{-1} is noticed. The absorption band at 1260 cm^{-1} is due to the CH$_3$ symmetric deformation of Si-CH$_3$. The absorption bands of Si-C stretching vibration and CH$_3$ rocking vibration occurred at 797 cm^{-1}. The spectrum of residual thin film on Ge prism reveals the absorption bands at 1260, 1016 and 797 cm^{-1} which can be observed in the spectrum of the hair as clearly be seen in Figure 4.13. Moreover, the spectrum also presents characteristic absorption bands of several ingredients in the region 3100-2800 and 1770-1330 cm^{-1}. Due to the low signal-to-noise ratio in these regions, these absorption bands cannot be identified.
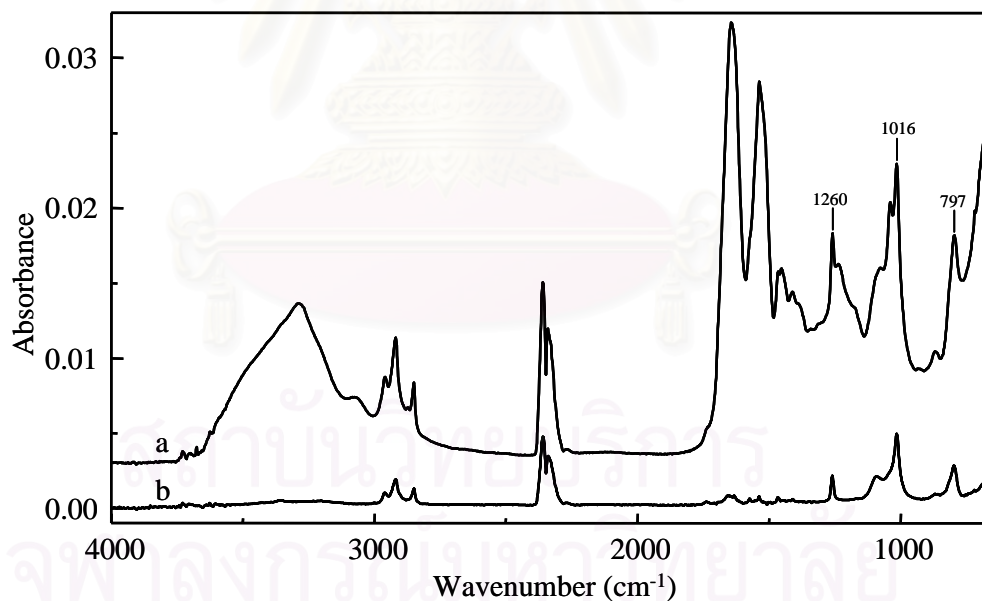
Figure 4.12 ATR spectra of conditioning cream-coated hair (a), residue on Ge IRE (b), acquired by the conventional ATR.
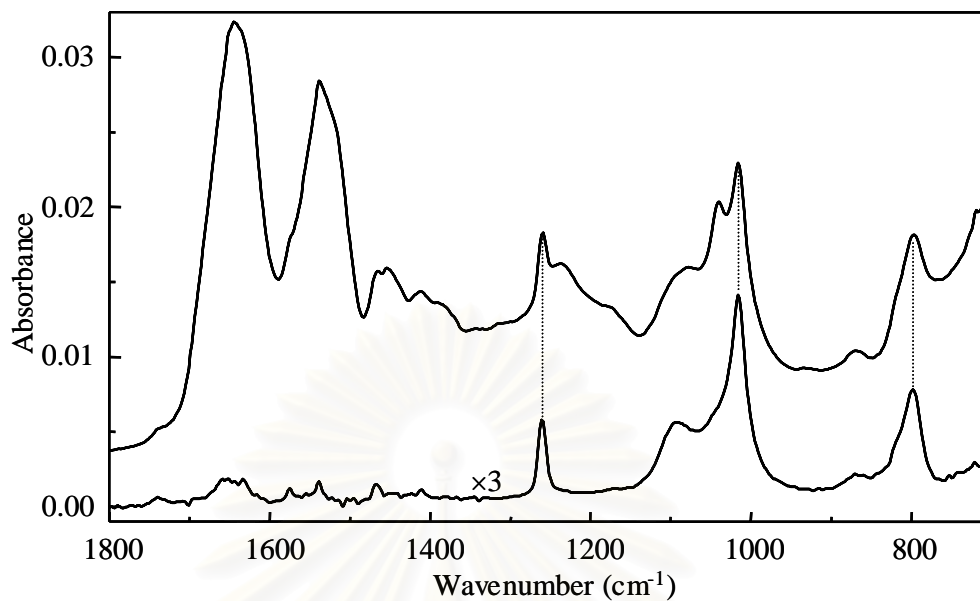
Figure 4.13 The magnified spectra in the 1800-700 cm^{-1} region of Figure 4.12.

By comparison, a single hair obtained from 3 women was investigated. Typical results are shown in Figures 4.14. The observed spectra show different spectral feature in the region 1350-950 cm^{-1}. This result assumed that the analyzing hair was treated with different shampoo and/or conditioning cream. Since the observed spectra acquired by the sharp-tip diamond µATR sensor were similar to that acquired by the conventional ATR with Ge IRE, the diamond µATR sensor can be employed for characterization of human hair and may utilize for forensic analysis.
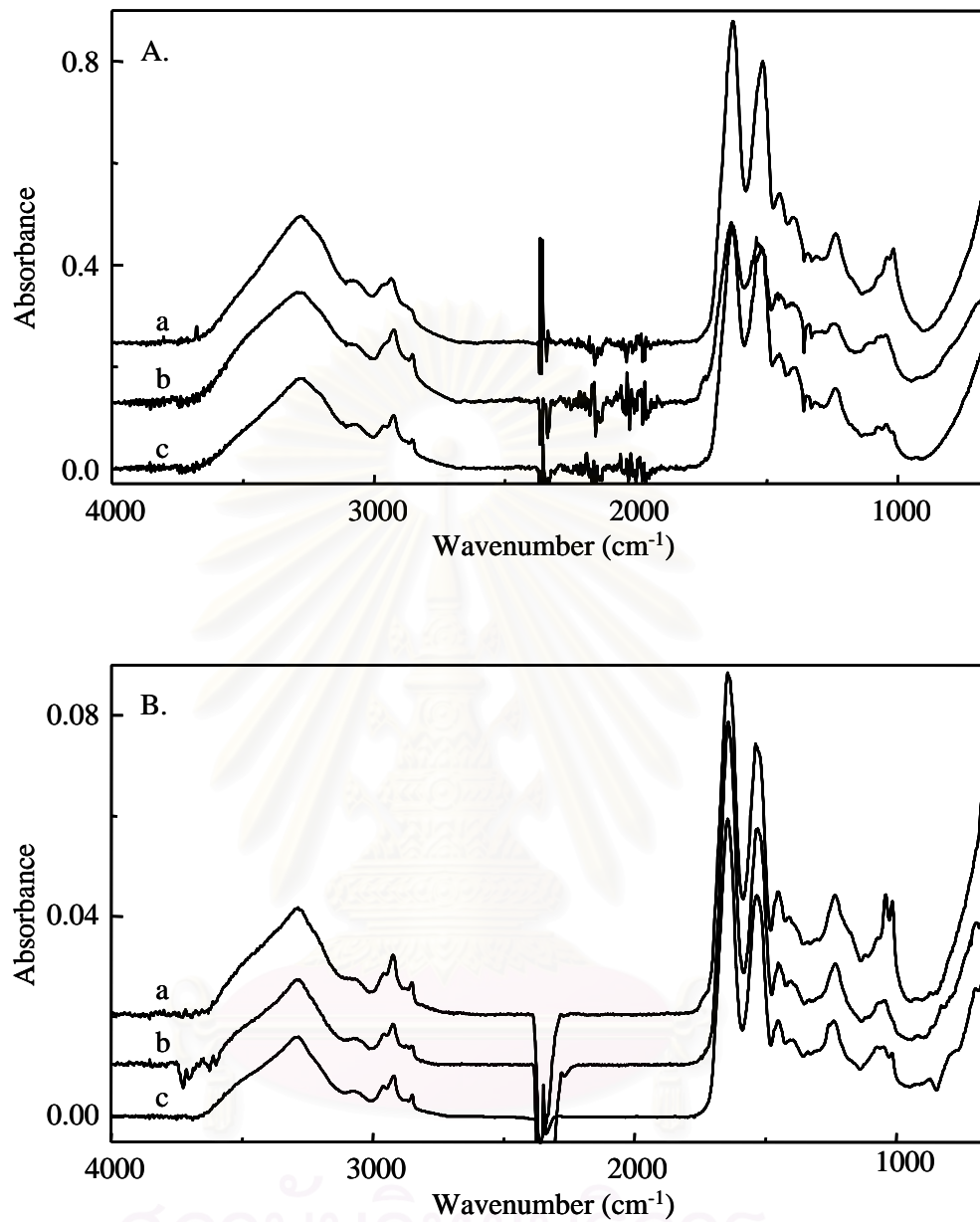
Figure 4.14   ATR spectra of a single hair from 3 women acquired by the sharp-tip
diamond µATR sensor (A) and the conventional ATR (B).

Table 4.3

ATR spectral assignments of human hair

Wavenumber (cm^{-1})		Assignments
diamond μATR sensor	conventional ATR	
3280	3290	O-H stretching mode of H$_2$O together with N-H stretching
2962	2960	Asym. CH$_3$ stretching
2930	2926	Asym. CH$_2$ stretching
2880	2878	Sym. CH$_3$ stretching
2853	2854	Sym. CH$_2$ stretching
1636	1645	Amide I C=O stretching and a small contribution from N-H bending
1520	1530	Amide II C-N stretching and N-H in-plane bending
1238	1238	Amide III N-H in-plane bending plus C-N stretching and contribution from O=C-N bending
1453	1453	C-H deformation
1399	1399	CH$_2$ and CH$_3$ bending
1121	1120	Sym. SO$_2$ stretching
1075	1177	SO stretching
1046	1048	S=O stretching

4.2.1.3 Silk fibers

Silk fiber consists of two major proteins, fibroin (body of silk fiber) and sericin (silk glue) which coated on silk fiber. The ATR spectrum of untreated silk acquired by the sharp-tip diamond μATR sensor is shown in Figure 4.15A(a). The observed spectrum of silk fiber shows typical absorption bands of amide I (1619 cm^{-1}), amide II (1514 cm^{-1}), and amide III (1233 cm^{-1}). The absorption band at 1443 cm^{-1} is due to the CH deformations. The absorption band at 1406 cm^{-1} is attributed to a CH_3 symmetric bending mode. The band at 1043 cm^{-1} is ascribed to the protein backbone stretching mode [39]. In general, degumming of silk fiber by alkali solutions allows to remove the soluble protein component, leaving the fibroin fiber core in almost pure form. The spectrum of alkali-treated silk fiber was also investigated as shown in Figure 4.15A(b). It should be noticed that the band at 1406 cm^{-1} disappears whereas the bands at 1409 and 1370 cm^{-1} appear. The absorption band around 1130-950 cm^{-1} appear significantly decrease intensity. A summary of band assignment of the silk fiber are shown in table 4.3.

The observed spectra of dyed silk fibers are illustrated in Figure 4.15A(c-e). Regarding these spectra, the absorption band at 1172, 998, and 979 cm^{-1} can be observed but these bands cannot be assigned what the accurate vibrational modes are. However, these obtained spectra show the different spectral features between untreated silk fiber, alkali-treated silk fiber, and dyed silk fiber. The observed spectra acquired by the sharp-tip diamond μATR sensor were similar to that acquired by the conventional ATR with Ge IRE (Figure 4.15B).
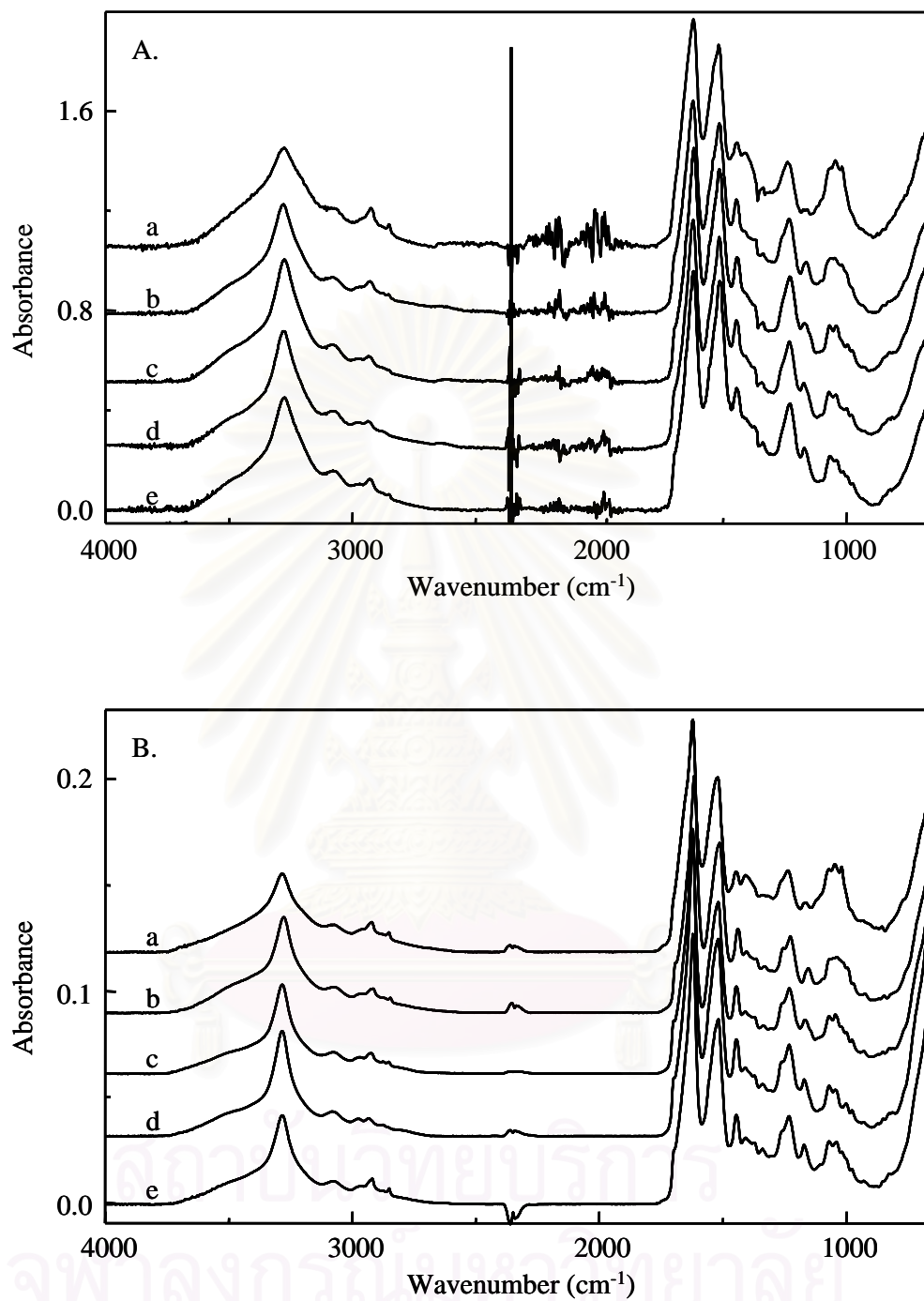
Figure 4.15 ATR spectra of untreated silk fiber (a), alkali-treated silk fiber (b), red silk fiber (c), green silk fiber (d), and blue silk fiber (e). the spectra were acquired by the sharp-tip diamond μATR sensor (A) and the conventional ATR (B).

Table 4.4

ATR spectral assignments of silk fiber

Wavenumber (cm^{-1})		Assignments
diamond μATR sensor	conventional ATR	
3278	3283	N-H stretching
2975	2964	Asym. CH_3 stretching
2930	2921	Asym. CH_2 stretching
2876	2874	Sym. CH_3 stretching
2854	2851	Sym. CH_2 stretching
1619	1621	Amide I
1514	1517	Amide II
1230	1231	Amide III
1108	1112	Sym. SO_2 stretching
1068	1071	SO stretching
1043	1044	S=O stretching

4.2.2 Synthetic fibers

4.2.2.1 Threads

The observed spectra of 4 different colors of thread samples that produced by a same manufacturer are shown in Figure 4.16. All obtained spectra show the same spectral feature which can assign as poly(ethylene terephthalate). Although, the poly(ethylene terephthalate) were treated with dyes, they have the same relative intensities of absorption bands. Due to very low concentration of the dye component on the thread surface, the different colored-threads cannot be distinguished. The observed spectra acquired by the sharp-tip diamond μATR sensor were similar to that acquired by the conventional ATR with Ge IRE (Figure 4.17).

Figure 4.16   ATR spectra of white thread (a), dark green thread (b), grey thread (c), and black thread (d), acquired by the sharp-tip diamond μATR sensor.

Figure 4.17   ATR spectra of the identical threads in Figure 4.16 in the 1800-750 cm^{-1} region.
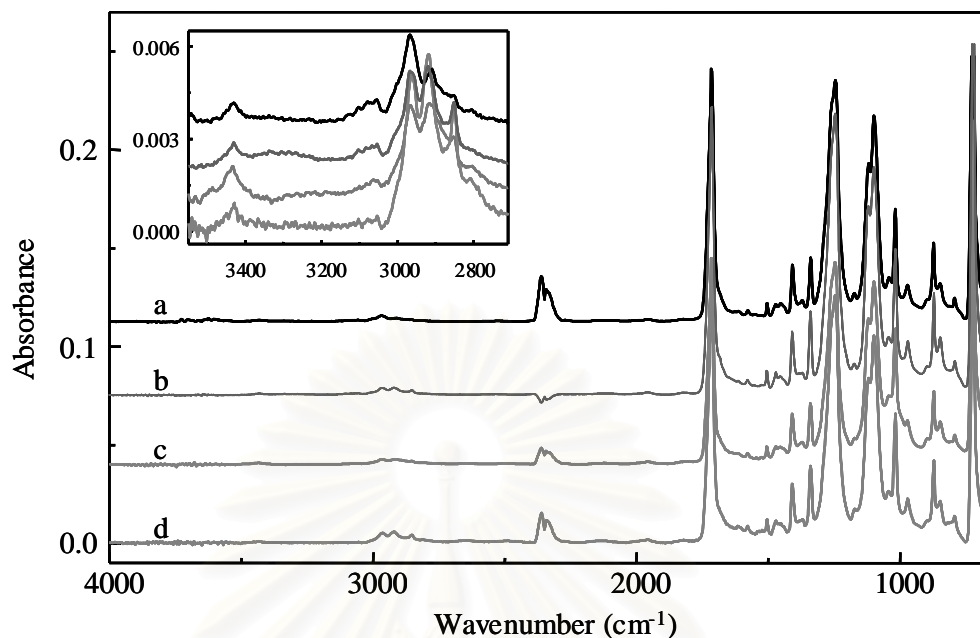
Figure 4.18   ATR spectra of white thread (a), dark green thread (b), grey thread (c), and black thread (d), acquired by the conventional ATR.

One of the important factors in forensic analysis is the capability to distinguish the similar sample. To investigate this aspect, the obtained spectra of 2 thread samples from different manufacture acquired by the sharp-tip diamond µATR sensor were compared as illustrated in Figure 4.19. Again, the obtained spectra show the features of poly(ethylene terephthalate). The spectra seem to be similar, however, there are differences in the relative intensities of absorption bands around 1800-750 cm^{-1}. It can be concluded that the thread from the different manufacture can be distinguished by diamond µATR technique. The observed spectra acquired by the sharp-tip diamond µATR sensor were similar to that acquired by the conventional ATR with Ge IRE (Figure 4.21).
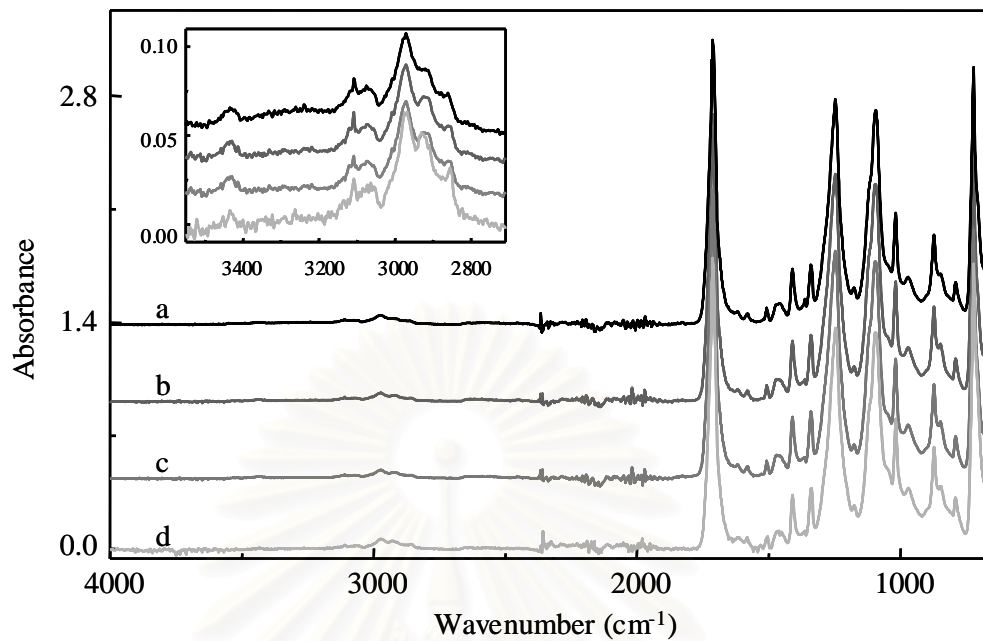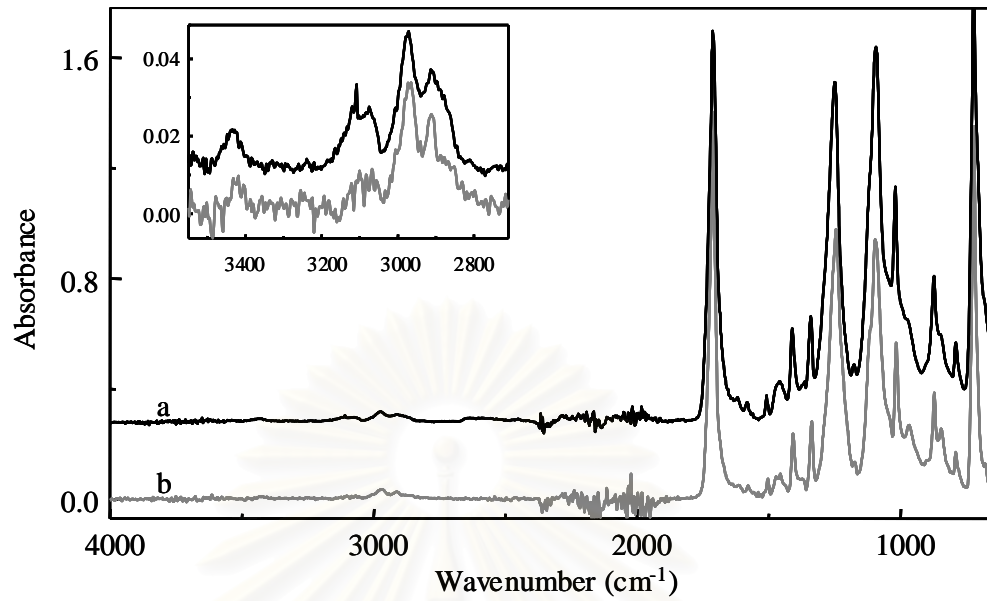
Figure 4.19 ATR spectra of threads from different manufacture acquired by the sharp-tip diamond μATR sensor.
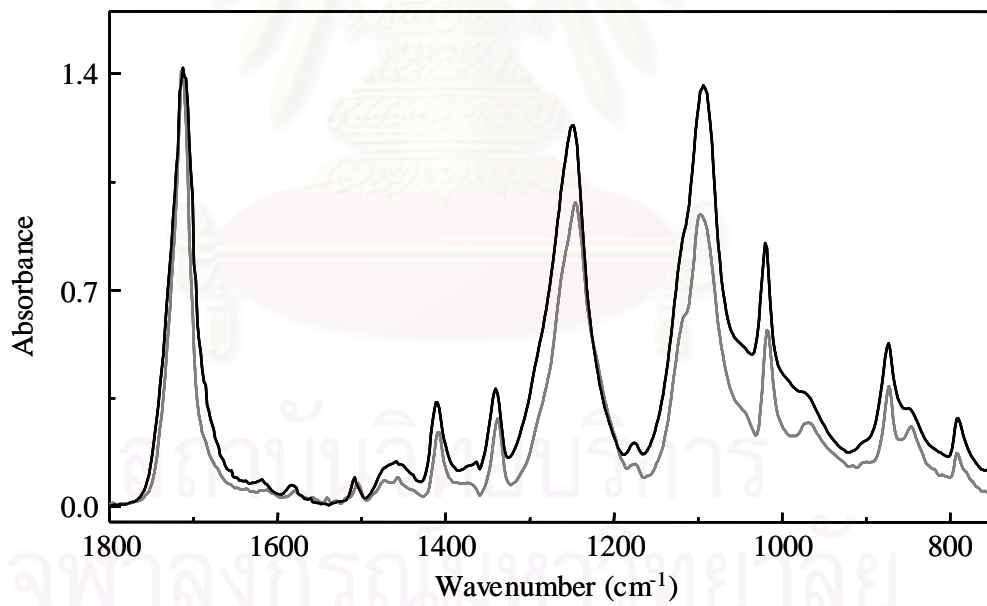
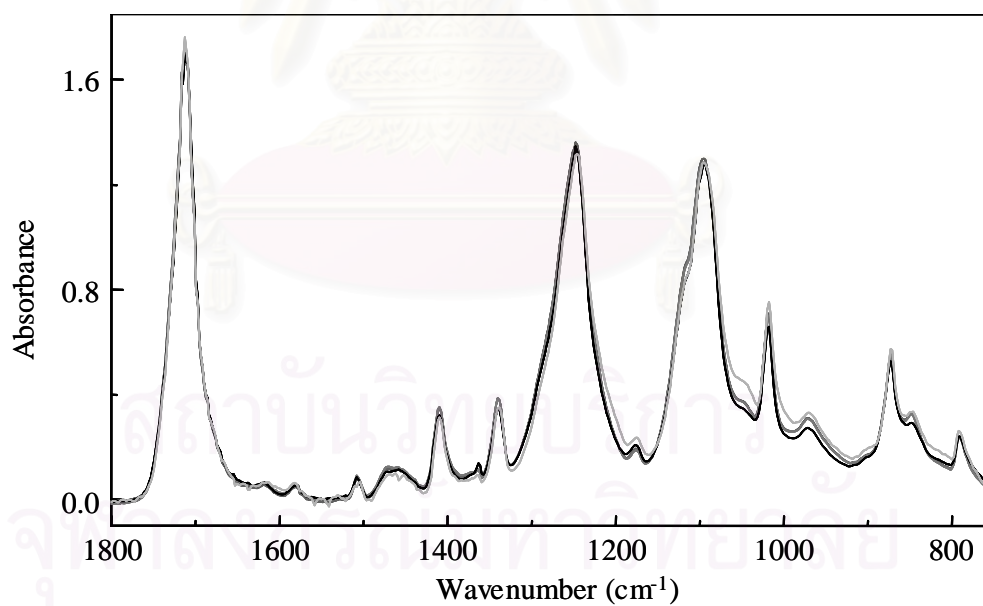**Figure 4.20** ATR spectra of the identical threads in Figure 4.19 in the 1800-750 cm^{-1} region.
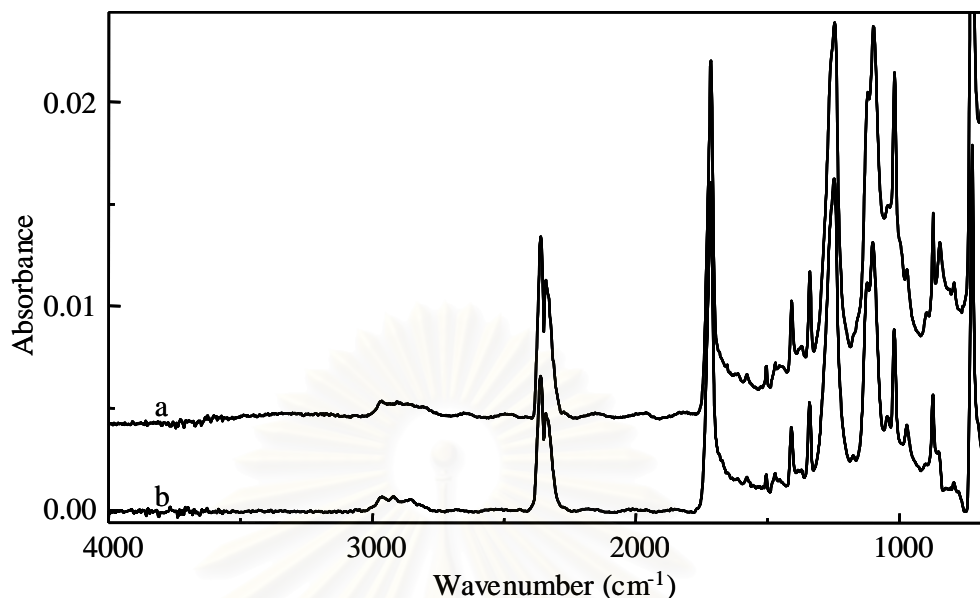
Figure 4.21 ATR spectra of threads from different manufacture acquired by the conventional ATR.

Considering all obtained spectra, most of the obtained spectra acquired by the novel diamond μATR sensor were similar to that acquired by the conventional ATR with Ge IRE. A small sample such as single fiber can be easily analyzed by using the novel diamond μATR sensor and conventional ATR. However, the rough surface of fiber may damage the surface of the Ge IRE in the conventional ATR technique when applying high pressure. The small culet and the hardness of the diamond IRE can eliminate the problems associated with the contact between the IRE and the fiber. One of the major drawbacks of the diamond IRE is the mask absorption band in the one-phonon region that can interfere in the obtained spectrum of the sample. However, the problem can be overcome by employing a diamond IRE with extremely low nitrogen content. The most advantage of using the novel diamond μATR sensor is economically of scale and trustworthy comparable to the Ge IRE in the conventional ATR technique.

CHAPTER V

CONCLUSIONS

ATR FT-IR spectroscopy is one of the powerful surface characterization techniques. A novel technique for ATR spectral acquisition by an infrared microscope with a gem quality round brilliant cut diamond as an IRE has been developed. The technique takes advantage of the total internal reflection phenomenon at the pavilion facet of the faceted diamond. By adjusting the table facet of the diamond IRE perpendicular to the incoming infrared beam, the infrared beam can be focused at the pavilion and the culet of faceted diamond for sharp-tip diamond IRE and flat-tip diamond IRE, respectively. Under the ATR experiment, transflected radiation is collected and the ATR spectrum provides spectral information associated with chemical species in the surface region where the evanescent field amplitude is still significant.

The novel homemade diamond μATR sensor was successfully employed to investigate the small sample such as single fiber. In this work, both natural fibers and synthetic fibers were studied. For the characterization of plant fiber, ATR FT-IR spectroscopy identifies the chemical structure and found that the coupling agent was localized at the surface of the fiber. Regarding the ATR spectra of human hairs, the observed spectra present the characteristic absorption bands of shampoo and conditioning cream on the surface of the human hairs. In the study of silk fiber, the observed spectra show the different spectral features among untreated silk fiber, alkali-treated silk fiber, and dyed silk fiber. In order to demonstrate of characterization of synthetic fiber, various color thread fibers were investigated by diamond μATR sensor. In the same manufacturer, the obtained ATR cannot be distinguished between different color treatments because the spectra show the same spectral feature and relative intensities. On the other hand, ATR spectra of thread fibers different manufactures show differences in the relative intensities. As a result, this technique can be employed from differentiation between the fibers from different manufacturers.

It is concluded that almost of the observed spectra acquired by the novel diamond μATR sensor were similar to that acquired by the conventional ATR with Ge IRE. Both techniques show potential for characterization of single fiber. Although the single fiber is small and its surface is not smooth, the surface information of the single fibers can be achieved. In the conventional ATR technique or accessory with Ge IRE, the system can not be achieved a good optical contact because it is always an air gap between the fiber and the IRE. A small air gap can significantly deteriorate the observed spectra. As a result, the technique is most effective for spectral acquisition of liquid or soft solid since an optical contact can be achieved. Moreover, this operation must be performed with extremely care since the excessive force might damage the surface of Ge IRE. Moreover, various commercial ATR accessories are very expensive while the homemade diamond μATR accessory is cost effective. The novel diamond ATR accessory can be used with all commercially available microscopes. The small culet and the hardness of the diamond IRE can eliminate the problems associated the contact between the IRE and the fiber. The high pressure can be applied onto the fiber against the diamond IRE in order to ensure the optimal contact during the spectral acquisition. Therefore, the spectral intensity that observed by the diamond IRE was about 10-folds of that obtained by the conventional ATR.

Suggestion for future work

The novel ATR technique not only shows the capability to characterize the small sample and/or small area but it also has many applications to perform with various samples. The surface characterization can be acquired by the flat-tip diamond IRE with an accurate optical contact.

The novel homemade diamond μATR sensor is probably employed for advanced analysis such as the forensic analysis, cosmetic industries, food packaging, textile technologies, and polymer industries due to the fast measured time, and less sample preparation. If the diamond with extremely low nitrogen content were employed as an IRE, the observed spectra in finger print region will be free of interference of the diamond absorption.

REFERENCES

1. Küpper, L.; Gulmine, J. V.; Janissek, P. R.; and Heise, H. M. Attenuated Total Reflection Infrared Spectroscopy for Micro-domain Analysis of Polyethylene Samples after Accelerated Ageing within Weathering Chambers. Vib. Spectrosc. 34 (2004): 63-72.

2. Monney, L.; Belali, R.; Vebrel, J.; Duois, C.; and Chambaudet, A. Photochemical Degradation Study of an Epoxy Material by IR-ATR Spectroscopy. Polym. Degrad. Stabil. 62 (1998): 353-359.

3. Gulmine, J. V.; Janissek, P. R.; Heise, H. M.; and Akcelrud, L. Degradation Profile of Polyethylene after Artificial Accelerated Weathering. Polym. Degrad. Stabil. 79 (2003): 385-397.

4. Ekgasit, S.; and Ishida, H. Application of a New Quantitative Optical Depth Profiling Technique for the Diffusion of Polymers. Appl.Spectrosc. 51(4) (1997): 461-465.

5. Ekgasit, S.; and Ishida, H. New Optical Depth-Profiling Technique by Use of the Multiple-Frequency Approach with Single ATR FT-IR Spectrum: Theoretical Development. Appl. Spectrosc. 51(10) (1997): 1488-1495.

6. Shick, R. A.; Koenig, J. L.; and Ishida, H. Theoretical Development for Depth Profiling of Stratified Layers Using Variable-Angle ATR. Appl. Spectrosc. 47(8) (1993): 1237-1244.

7. Belfer, S; Leiberich, R.; Urison, Y. and Kadem, O. Surface Characterization by FTIR-ATR Spectroscopy of Polyethersulfone Membranes-Unmodified, Modified and Protein Fouled. J. Membrane Sci. 172 (2000): 113-124.

8. Abdelmouleh, M.; Boufi, S.; Belgacem, M. N.; Duarte, A. P.; Salah, A. B.; and Gandini, A. Modification of Cellulic Fibers with Functionalised Silanes: Delvelopement of Surface Properties. Int. J. Adhes. Adhes. 24 (2004): 43-54.

9. Enlow, E. M.; Kennedy, J. L.; Nieuland, A. A.; Hendrix, J. E.; and Morgan S. L. Discrimination of Nylon Polymers Using Attenuated Total Reflection Mid-infrared Spectra and Multivariate Statistical Technique. Appl. Spectrosc. 59(8) (2005): 986-992.

10. Garside, P.; and Wyeth, P. Identification of Cellulosic Fibers by FTIR Spectroscopy: Thread and Single Fiber Analysis by Attenuated Total Reflectance. Stud. Conserv. 48(4) (2003): 269-275.

11. Harrick, N. J. Surface Chemistry from Spectral Analysis of Totally Internally Reflected Radiation. J. Phys. Chem. 64 (1960): 1110-1114.

12. Fahrenfort, J. Attenuated Total Reflection a New Principle for the Production of Useful Infrared Reflection Spectra of Organic compounds. Spectrochim. Acta. 17 (1961): 698-709.

13. Harrick, N. J. (Ed.). Internal Reflection Spectroscopy. New York: Harrick Scientific Corporation, 1979.

14. Skourlis, T. P.; and McCullough, R. L. Measurement of Diffusivity of Liquid Diamine in Solid Expoxies Using Attenuated Total Reflectance Spectroscopy (FTIR-ATR). J. Appl. Polym. Sci. 52 (1994): 1241-1248.

15. Buffeteau, T.; Desbat, B.; and Eyquem, D. Attenuated Total Reflection Fourier Transform Infrared Microspectroscopy: Theory and Application to Polymer Samples. Vib. Spectrosc. 11 (1996): 29-36.

16. Balik, C. M.; and Simendinger III, W.H. An Attenuated Total Reflectance Cell for Analysis of Small Molecule Diffusion in Polymer Thin Films with Fourier-transform Infrared Spectroscopy. Polymer 39(20) (1998): 4723-4728.

17. Milosevic, M.; Sting, D; Rein, A. Technical Note: Diamond-Composite Sensor for ATR Spectroscopy. Spectroscopy 10(4) (1995): 44-49.

18. Coates, J. P. A New Universal Sampling Tool for Infrared Spectroscopy Spectroscopy Showcase 16 (1997): 18-20.

19. Coates, J. P. A Diamond Based Sampling Accessory for Solid and Liquid Sampling in Infrared Spectroscopy Amer. Lab. April (1997): 22C-22J.

20. Ekgasit, S.; and Thongnopkun, P. Novel ATR FT-IR Microscopy Using a Gem Quality Diamond as an Internal Reflection Element. <u>Appl. Spectrosc.</u> 59 (2005): 1236-1241.

21. Urban, M. W. (Ed.). <u>Attenuated Total Reflectance Spectroscopy of Polymer: Theory and Practice</u>.   Washington, DC: American Chemical Society, 1996.

22. Ekgasit, S.; and Siesler, H. W. Simplified Equation for ATR Spectral Intensity of a Three-Phase System. <u>Appl. Spectrosc.</u> 52(3) (1998): 367-374.

23. Hemphill, T. C.; Reinitz, I. M.; Johnson M. L.; and Shigley, J. E. Modeling the Appearance of the Round Brilliant Cut Diamond: An Analysis of Brilliance. <u>Gem.Gemol.</u> 34(3) (1998): 158-183.

24. Reinitz, I. M.; Johnson M. L.; Hemphill, T. C.; Gilbertson, R. H.; Geurts, R. H.; and Green, D. B. Modeling the Appearance of the Round Brilliant Cut Diamond: An Analysis of Fire, and More about Brilliance. <u>Gem.Gemol.</u> 37 (2001): 174-197.

25. Ekgasit, S.; and Thongnopkun, P. Transflectance Spectra of Faceted Diamonds Acquired by Infrared Microscopy. <u>Appl. Spectrosc.</u> 59 (2005): 1160-1165.

26. Katon, J. E. Infrared Microspectroscopy. A Review of Fundamentals and Applications. <u>Micron</u> 27 (1996): 303-314.

27. Tserki, V.; Zafeiropoulos, N. E.; Simon, F.; and Panayiotou, C. A Study of Acetylation and Propionylation Surface Treatment on Natural Fibers. <u>Composites Part A</u> 36 (2005), 1110-1180.

28. Herrera-Franco, P. J.; and Valadez-González, A. A Study of the Mechanical Properties of Short Natural-Fiber Reinforced Composites. <u>Composites Part B</u> 36 (2005): 597-608.

29. Valadez-Gonzalez, A.; Cervantes-Uc, J. M.; Olaya, R.; and Herrera-Franco, P. J. Chemical Modification of Henequén Fibers with an Organosilane Coupling Agent. <u>Composites Part B</u> 30 (1999): 321-331.

30. Valadez-Gonzalez, A.; Cervantes-Uc, J. M.; Olaya, R.; and Herrera-Franco, P. J. Effect of Fiber Surface Treatment on Fiber-Matrix Bond Strength of Natural Fiber Reinforced Composites. Composites Part B 30 (1999): 309-320.

31. Rong, M. Z.; Zhang. M. Q.; Liu, Y.; Yang, G. C.; and Zeng, H.M. The Effect of Fiber Treatment on the Mechanical Properties of the Unidirectional Sisal-Reinforced Epoxy Composite. Compos. Sci. Technol. 60 (2001): 1437-1447.

32. Matuana, L. M. Influence of Interactions on the Properties of PVC/Cellulosic Fiber Composites. Polym. Composites 19(4) (1998): 446-455.

33. Cantero, G.; Arbelaiz, A.; Llano-Ponte, R.; and Mondragon, I. Effect of Fiber Treatment on Wettability and Mechanical Behavior of Flax/Polypropylene Composites. Composi. Sci. Technol. 63 (2003): 1247-1254.

34. Mohanty, A. K.; Khan, M. A.; and Hinrichsen, G. Surface Modification of Jute and Its Influence on Performance of Biodegradable Jute-Fabric/Biopol Composites. Compos. Sci. Technol 60 (2000): 1115-1124.

35. Edwards, H. G. M.; Farwell, D. W.; and Webster, D. FT Raman Microscopy of Untreated Natural Plant Fibers. Spectrochim. Acta A 53 (1997): 2383-2392.

36. Akhtar, W.; Edwards, H. G. M.; Farwell, D. W.; and Nutbrown, M. Fourier-transform Raman Spectroscopic Study of Human Hair. Spectrochim. Acta A 53 (1997): 1021-1031.

37. Panayiotou, H.; and Kokot, S. Matching and Discrimination of Single Human-Scalp Hairs by FI-IR Micro-Spectroscopy and Chemometrics. Anal. Chim. Acta 392 (1999): 223-235.

38. Lyman, D. J.; and Murray-Wijelath, J. Fourier Transform Infrared Attenuated Total Reflection Analysis of Human Hair: Comparison of Hair from Breast Cancer Patients with Hair from Healthy Subjects. Appl. Spectrosc. 59(1) (2005): 26-32

39. Taddei, P.; Montri, P.; Freddi, G.; Arai, T.; and Tsukada, M. IR Study on the Binding Mode of Metal Cations to Chemically Modified *Bombyx mori* and Tussah Silk Fibers. J. Mol. Struct. 651-653 (2003): 433-441.

CURRICULUM VITAE

Miss Ruechuwee Meechue

1981	Born	: September, 17th in Surin, Thailand
	Father	: Mr. Sukhum Meechue
	Mother	: Mrs. Sucheera Meechue

1994   Primary School (Prasatsuksakarn School, Surin)

2000   High School (Sirindhorn School, Surin)

2004   Bachelor of Science (Chemistry),
Kasetsart University, Bangkok

2006   Master degree, Program in Petrochemistry and Polymer Science, Faculty of Science, Chulalongkorn University, Bangkok